3-9-2009

Modeling Thermal Inactivation of Bacillus Spores

Emily A. Knight

MODELING THERMAL INACTIVATION OF *BACILLUS* SPORES

THESIS

Emily A. Knight
Captain, USAF

AFIT/GAM/ENC/09-01

DEPARTMENT OF THE AIR FORCE
AIR UNIVERSITY

AIR FORCE INSTITUTE OF TECHNOLOGY

Wright-Patterson Air Force Base, Ohio

The views expressed in this thesis are those of the author and do not reflect the official policy or position of the United States Air Force, Department of Defense, or the United States Government.

AFIT/GAM/ENC/09-01

MODELING THERMAL INACTIVATION OF *BACILLUS* SPORES

THESIS

Presented to the Faculty

Department of Mathematics and Statistics

Graduate School of Engineering and Management

Air Force Institute of Technology

Air University

Air Education and Training Command

In Partial Fulfillment of the Requirements for the

Degree of Master of Science

Emily A. Knight, BA

Captain, USAF

March 2009

AFIT/GAM/ENC/09-01

MODELING THERMAL INACTIVATION OF *BACILLUS* SPORES

Emily A. Knight, BA
Captain, USAF

Approved:

/signed/	20 March 2009
Dr. William P. Baker (Chairman)	Date
/signed/	20 March 2009
Dr. Larry W. Burggraf (Member)	Date
/signed/	20 March 2009
Maj. Kyle A. Novak (Member)	Date

Abstract

This research models and analyzes methods to damage *Bacillus* spores through various heat-treatments. AFIT researchers have been examining and developing methods to characterize the effects of heating *Bacillus anthracis* spores to high temperatures and for short durations. The current laboratory experiment being conducted is designed to imitate the neutralization of *Bacillus* spores by a thermal pulse similar to that of a conventional weapon detonation. The research contained in this report designs a thermal model that replicates the current laboratory experiment and evaluates the rate of thermal diffusion throughout the *Bacillus* spores.

In addition, a micro-model of the effects of dry and wet heating on a spore is presented. By applying heat to a spore, we energize adsorbed, absorbed, and chemically bound water molecules. These energized molecules have greater mobility and diffusion within the spore, as well as between the spore and the surrounding environment. The water release permits hydrolysis reactions to take place with the spore's DNA and other proteins. These chemical reactions degrade the DNA and proteins to such an extent that the DNA cannot be repaired or replicated, thus causing spore death. We further assert that damage to a spore is based on a certain initial DNA information content and the spore population's protein 'fitness'. Once this protein fitness level is degraded below a critical threshold, the protein can no longer repair DNA and thus the spore is unable to germinate, or produce outgrowth. These assertions allow us to create a probability of kill model based on water mobility, hydrolysis, a spore's DNA information content, and the spore population's protein fitness.

Acknowledgements

I would like to thank my husband and family for their unfailing encouragement and support, my peers for never turning me away when I needed help, my committee members, Dr. Baker, Dr. Burggraf, and Maj. Novak, for their enduring patience and willingness to teach, and finally my advisor, Dr. Baker, for showing me just a few of the interesting and important applications that mathematics has within the real world.

Emily A. Knight

Table of Contents

Page

List of Figures

List of Tables

MODELING THERMAL INACTIVATION OF *BACILLUS* SPORES

I. Introduction

1.1 Background

In 1979, in Sverdlovsk, Russia, a Soviet bioweapons facility unintentionally released spores of *Bacillus anthracis (B.a.)*, the bacterium that causes anthrax. This led to an epidemic of inhalational anthrax in Russia and 18 cases of exposure to anthrax in the United States (U.S.). In 1995, a Japanese cult, Aum Shinrikyo, released aerosols of anthrax and botulism throughout Tokyo and within the Tokyo subway system at least eight times. Although the strain of dispersed anthrax was used for animal vaccinations and was not significantly dangerous to humans, the attacks produced widespread panic. In 2001, following the terrorist attacks of 11 September, *B.a.* spores were mailed through the U.S. Postal Service to members of the U.S. Senate and to national news agencies. These biological attacks resulted in 22 combined inhalational and cutaneous cases of anthrax infection. Of these 22 cases, five Americans died and "the nation was terrorized in what became the worst biological attacks in U.S history" [3]. These attacks illustrated the prevalent need of the U.S. to consider the detection, recognition, environmental surveillance, decontamination, and destruction of anthrax.

The Working Group on Civilian Biodefense identified anthrax as a biological agent that may be used as a weapon and "in worst case scenarios, could cause disease and deaths in sufficient numbers to gravely impact a city or region". At least 13 countries are suspected to contain offensive biological weapons programs [4]. Therefore, both political and military factions within the U.S. have stressed the need for counter terrorism weapons and biodefensive systems capable of destroying biological and chemical weapons [47].

1.2 Purpose of the Research

Although multiple data sources can be found regarding dry heat damage to spores over long periods of time, very little research has been completed on extremely short duration exposures consistent with detonation of a conventional weapon. Also extremely important is understanding the effectiveness of weapons against biological targets. Researchers at the Air Force Institute of Technology (AFIT), working in conjunction with the Air Force Nuclear Weapons and Counterproliferation Agency (AFNWCA), has been researching and developing methods to characterize the effects of heating *Bacillus anthracis* spores to high temperatures and for short durations. The current laboratory experiment being conducted by AFIT researchers is designed to replicate the neutralization of *B.a.* spores by a thermal pulse similar to that of weapon detonation. Specifically, the objective of the experiment is to determine the probability of kill for *B.a.* spores exposed to high temperatures, 300 to 1300 °K (27 to 1027 °C), for short duration exposures, 0.01 to 3 seconds [5]. The experiment consists of rastering a solid state laser (Nd:YAG laser) beam to indirectly heat the spores for various time intervals and temperature ranges using a laboratory produced, custom black body radiator. The spores are analyzed before and after the laser heating to determine the probability of kill dependent on regeneration of each spore. In order to accurately predict the effectiveness of the laser heating method, it is necessary to understand how the thermal pulse (generated by the laser) propagates through the test apparatus. To accomplish this, a thermal model will be designed to replicate the current laboratory experiment and evaluate the rate of thermal diffusion throughout the *B.a.* spores. This model will be numerically evaluated.

Once the thermal exposure is understood, it will be necessary to characterize the influence this has on the spore itself. There have been many proposed models regarding heat damage to spores which are briefly summarized here. Setlow theorizes that DNA damage is the primary cause of thermal damage because the target for dry heat treatment "is at least in part DNA, as there is... much DNA damage and loss of DNA repair capacity" [39]. Jagannath, Tsuchido, and Membré speculate

that heating spores that are suspended in certain foods is more efficient due to the existence of acidic pH [24]. Geeraerd, Herremans, and Van Impe hypothesize that the components within the spores experience a log linear inactivation and the spores themselves encounter a $\log_{10}$ rate of thermal decay. Casolari assumes a spore is killed by a "lethal hit of a water molecule" due to the high amount of energy that water molecules contain [18]. One contention that all these models have in common is that spores are extremely resistant to both wet and dry heat. They also agree that while dry heat damage is caused by at least some DNA damage, wet heat does not produce any DNA damage.

We have discussed models which theorize damage to *Bacillus* spores by various methods. These models use multiple *Bacillus* species such as *anthracis, cereus,* and *subtilis*. Therefore, it is necessary to discuss the validity of using different species to characterize spore damage due to heat treatment. One of the obvious concerns in regards to heat damage is varying spore heat resistance between species but "these mechanisms appear to be conserved across *Bacillus* species" [40]. All species of the *Bacillus* genus are genetically similar with the exception of the existence of an outer spore layer called an exosporium. But the exosporium is not believed to provide increased protection for the spore [21]. For these reasons, we assume that spore kill mechanisms are similar across the *Bacillus* genus.

The approach of this research focuses on hydrolysis reactions within the spore. Hydrolysis is a reaction of a molecule with water. In this case, water can react with biopolymers such as DNA and proteins resulting in depolymerization (breaking a large strand of polymers into two smaller ones) or removal of a side group of the polymer [27]. We propose that these hydrolysis reactions decimate the levels of DNA and proteins to such an extent that the DNA can no longer be repaired. This, in turn, prevents the spore from germination and effectively kills the spore. In order to assess the probability of kill, a water production-diffusion micro model based on hydrolysis reactions is needed to determine thermal damage to *Bacillus* spores. The hydrolysis reactions occur mainly in the cortex and the core of each spore and since

the water molecules are assumed to be mobile, this model will focus on diffusion of water throughout each section of the spore in relation to ambient water concentration. The ambient water concentration is dependent on whether the spore is being heated via wet or dry heat. A wet heating process is one in which the spore is suspended in a saturated aqueous environment while a dry heating process applies hot air, which contains little to no water vapor, to the spore. Either heating process will energize water molecules contained in a spore and these energized molecules become mobile. The consequence of an increase in core water content is "more rapid heat inactivation of spore core proteins" [11]. Our model will consider the production-diffusion of water throughout the spore and relate it to the rate of hydrolysis reactions with DNA and proteins. Finally, a probability of kill model that relates the damage of the initial DNA information content to the decimation of the spore population's protein 'fitness' will be presented.

1.3 Research Objectives

- Numerically model the current AFIT experiment of heating *B.a.* spores and the rate of thermal diffusion throughout the spores in order to calculate the actual temperature and durations experienced
- Analytically model and analyze the micro-level damage within a *B.a.* spore due to production, diffusion, and hydrolysis reactions of water molecules throughout a spore.
- Relate the thermal model to production/diffusion/hydrolysis reaction model to develop a probability of kill model based on the threshold killing mechanisms of *B.a.* spores

1.4 Overview

The objectives previously defined will be presented in the following manner. The development, numerical methods, and results of the thermal model will be described

in Chapter II. Chapter III explains the release of water molecules within the spore due to heat application. It illustrates the diffusion of these water molecules throughout the spore which promotes hydrolysis reactions to occur. Chapter IV discusses our proposal that spore damage is caused by hydrolysis reactions since hydrolysis will damage a spore's DNA information content and degrade repair proteins to such an extent that the DNA cannot be repaired. It will describe and present results from the kill probability model. The conclusion, as well as any suggested future work, will be contained in Chapter V.

II. Thermal Model and Analysis

2.1 Current Experiment

In order to analyze the consequences of high temperatures for short durations on *Bacillus anthracis*(*B.a.*), researchers at AFIT have developed multiple laboratory experiments consistent with detonation of a conventional weapon. This research will numerically model the heating and thermal diffusion created by the current experiment. To understand the thermal model developed by this research, a thorough description of the experiment is required.

The current experiment was created to heat *B.a.* spores using a solid state, Nd:YAG laser. A soda lime glass coverslip was micro-etched to generate wells in the coverslip. The circular wells were 50 *microns* (μm) wide, between 3 and 5 μm deep, and each coverslip contained a grid of 532 total wells (38 columns by 14 rows). See Figure 2.1 for a top-level view of the etched coverslip [20].

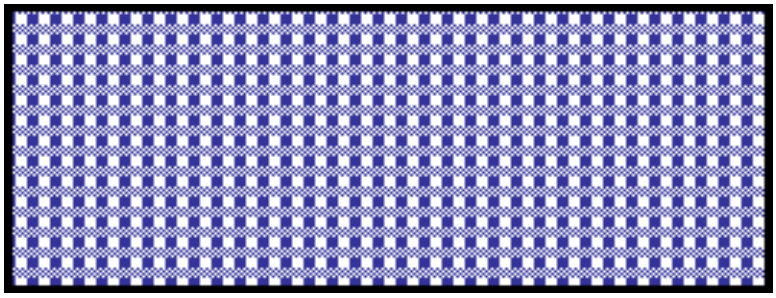

Figure 2.1: Etched Coverslip

The wells were then populated with the *B.a.* spores. The diameter of a *B.a.* spore is approximately 1 μm [38]. Viable wells contained between 1 and 15 spores each. A soda lime glass slide was also micro-etched with wells. Carbon black was placed in these wells as a optical absorber. Because the spores could not be directly heated via the laser, the carbon black served as a 'hot plate' converting optical energy to thermal energy and conducting heat into the spore wells. The carbon black wells were approximately 75 μm wide to ensure complete coverage of the wells containing

the spores (50 μm wide). There are 1500 μm between each carbon black well in each column, row, and from all edges of the coverslip. The glass slide was then placed over the etched coverslip holding the spores. The slide with the carbon black wells was removed after heat treatment so the spores could be viewed under the microscope. See Figure 2.2 for a visualization of the experiment (not drawn to scale). This figure gives a spliced view of the test mechanism with an illustration of the two glass layers. The spores wells are directly beneath the sections of carbon black which are 1500 μm apart. The laser heats the carbon black which then emits heat to the spores.

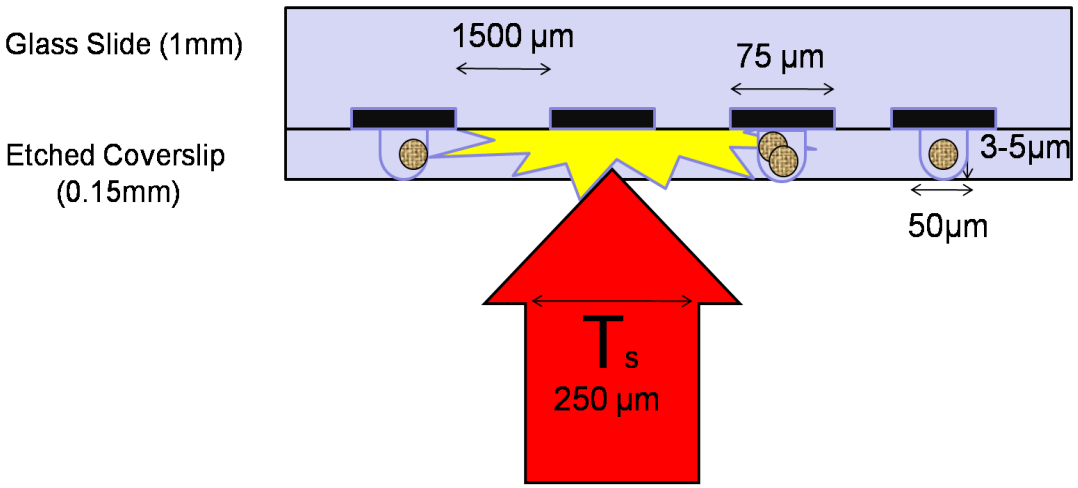

Figure 2.2: Visualization of Experiment

The spores were heated against the carbon black wells via a Nd:YAG laser which was operated at different powers in order to vary the temperatures experienced by the spores. The laser beam was rastered across each column and row of the test apparatus. The heating times were controlled by adjusting the raster rate of the sample relative to the laser beam. Immediately following the heat treatment, the *B.a.* spores were counted using a Zeiss microscope and allowed to incubate and grow. "Growth rates are less a function of the organism and more that of the sample's original preparation and the environmental conditions of that preparation; temperature, moisture content, pH" [5]. Ideal growth times, based on the organisms used, fluctuated between three

and five hours. Therefore, the spores were allocated a growth period of three hours and were again viewed and counted via the Zeiss microscope.

Now armed with an appreciation of the general experiment, it is necessary to understand which parameters of the experiment are to be modeled. As one of the research objectives is to evaluate the rate of thermal diffusion propagated throughout the *B.a.* spores, the numerical model will only take into consideration the thermal heating of one spore well. The model will illustrate the thermal heating throughout the coverslip and slide and will take into account the rate of heat diffusion from the center of one spore well to approximately halfway in between this spore well and the adjacent spore well. The boxed region shown in Figure 2.3 illustrates the model area of concern (not drawn to scale).

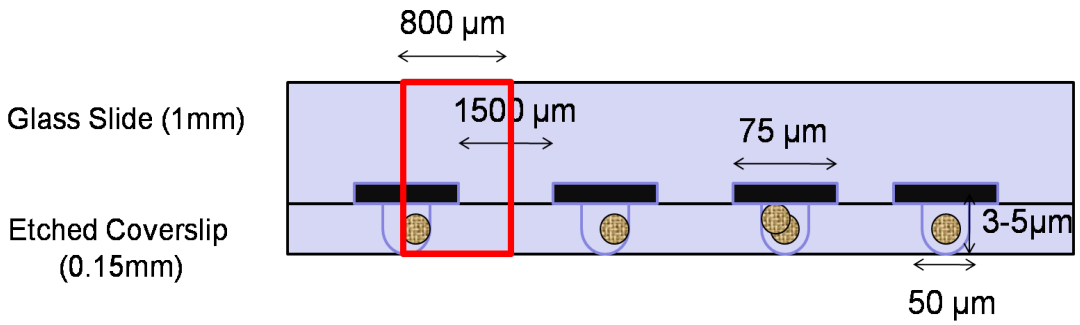

Figure 2.3: Area of Experiment to be Modeled

2.2 Model With Respect to Experiment

2.2.1 Heat Equation.

This research is concerned with the rate at which the *B.a.* spores directly beneath the carbon black are heated and the influence this heating has on adjacent spores. In other words, does the adjacent spore realize any significant thermal energy from the previously heated carbon black well? To answer these questions, we consider

the thermal diffusion equation as given by:

$$\rho C \frac{\partial T}{\partial t} = \nabla \cdot K \nabla T + S \tag{2.1}$$

where

$$T = \text{temperature}$$
$$t = \text{diffusion time}$$
$$C = \text{specific heat}$$
$$\rho = \text{density}$$
$$K = \text{thermal conductivity}$$
$$S = \text{a distributed heat source.}$$

In relation to the experiment, our source has a power density proportional to the Nd:YAG laser intensity and its units are W/cm^2. See Table 2.1 for the properties of soda lime glass used in the experiment [42].

Table 2.1: Properties of Soda Lime Glass

Property	Value	Units
C	.879	J/g°C
ρ	2.44	g/cm^3
K	0.94×10^{-2}	W/cm°C
$\kappa = \frac{K}{\rho C}$	0.438×10^{-2}	cm^2/sec

Because the spore wells and the carbon black are uniformly spaced and each is circularly symmetric, we can consider the model area to be a three dimensional cylindrical volume. As such, we will be evaluating the heat equation in cylindrical coordinates. Further, we assume the material is homogeneous, isotropic, and has no angular dependence. Thus, the model is reduced to axis symmetric and two dimensional with respect to the radial direction and throughout the thickness of the

apparatus. Therefore, Equation (2.1) becomes:

$$\frac{\partial T}{\partial t} = \kappa \frac{1}{r} \frac{\partial}{\partial r}(r \frac{\partial T}{\partial r}) + \kappa \frac{\partial^2 T}{\partial^2 z} + \frac{S}{\rho C} \tag{2.2}$$

where r is the radial distance and z is the distance through the thickness of the test apparatus.

2.2.2 Carbon Black.

Lamp black has an emissivity of $\epsilon = 0.98$. As such, we will assume carbon black to be a perfect black body absorber. A black body absorbs all light that falls onto it and emits as much thermal energy as it absorbs [10]. No light passes through a black body and none is reflected. These properties make the region of carbon black an ideal source of thermal energy. In the experiment, the carbon black region is the only source of the thermal energy that heats the region of the spores through conduction. Refer to Figure 2.4(d) to view the carbon black immediately after heat treatment.

2.2.3 Source Term.

The heat source is produced by the Nd:YAG laser beam. The beam has a circular Gaussian distribution with a half-power beam-width of 250 μm in diameter. Therefore, if the beam is centered on an absorber well, the heat source is nearly uniform across the carbon black well. The laser provides the radiant energy which the carbon black absorbs. Due to experimental limitations, the carbon black wells were not populated equally with carbon. This reduction in carbon black diminishes the efficiency of a given carbon black well. Refer to Figure 2.4 for microscopic views of the carbon black wells. Only the wells that were filled 85% (see Figure 2.4(b)) to 100% (see Figure 2.4(c)) with carbon black were used as viable wells for the experiment. Since the experiment only took into account those carbon black wells that were populated by at least 85%, and because the wells were only 75 μm wide, the laser beam was sufficiently large enough to assume a uniform illumination. This leads to uniform

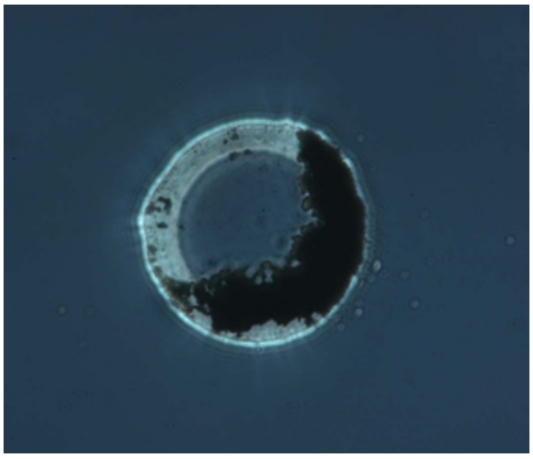

(a) Carbon Black well that was barely filled and thus not considered a viable well for the experiment.

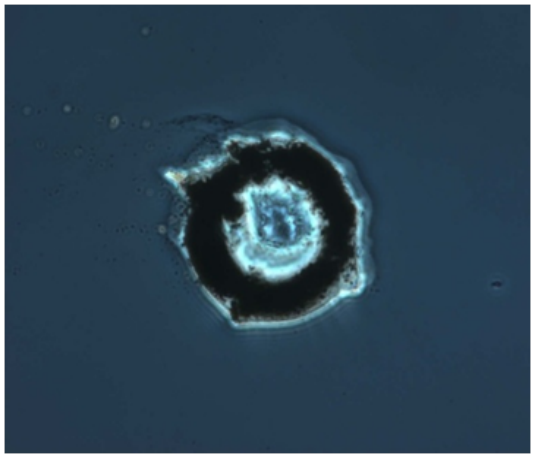

(b) Carbon black well filled by at least 85%.

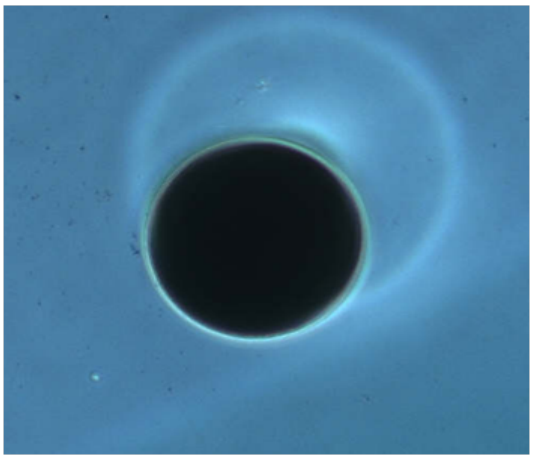

(c) Perfectly filled carbon black well.

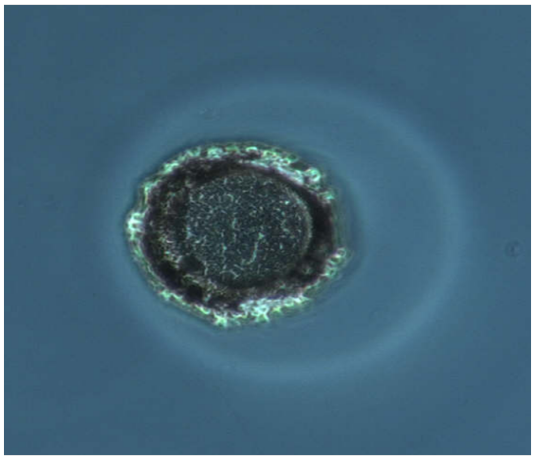

(d) Completely filled carbon black well viewed after heat treatment.

Figure 2.4: Carbon black wells as viewed underneath the Zeiss microscope [5].

source in the carbon black region proportional to the laser power and the volume of the deposited carbon. Further, the source is assumed to either be on or off and only exists in the carbon black region. The reason for this is that the glass is assumed to be a perfectly non-absorbing medium, hence a totally ineffective radiator. This is a good assumption for our temperatures of interest. For example, the difference between hot and cool glass at 600 °C cannot be seen but it can be seen at 1000 °C. For this reason we model the source as

$$S(t) = \begin{cases} kP, & \text{laser on} \\ 0, & \text{laser off} \end{cases}$$

where P is the laser power in Watts and k is the proportionality constant (this is determined during laboratory calibration).

2.2.4 Boundary Conditions.

The boundary conditions need to imitate the laboratory experiment as closely as possible. As shown by Figure 2.3, the left-hand boundary of the model area is the center of the carbon black and spore wells. By the axisymmetric assumption, there will be no heat flux across this boundary as heat must flow outward from the wells. Therefore, we will impose the condition

$$\frac{\partial T}{\partial r}(r, z, t)\bigg|_{r=0} = 0. \tag{2.3}$$

The test apparatus is held together by clamps at the corners of the slides and suspended in air to allow rastering of the laser. Therefore, at the top and the bottom of the slide, the boundary condition allows for convective heat transfer through air. In other words, the "flux across the surface is proportional to the temperature difference between the surface and the surrounding medium" [9]. We will use Newton's law of cooling to describe this heat transfer from the surface of the slides to the surrounding

air. This leads to the equations

$$-K\frac{\partial T}{\partial z} = h(T - T_s) \mid_{z=z_{\text{top}}} \tag{2.4}$$

and

$$K\frac{\partial T}{\partial z} = h(T - T_s) \mid_{z=z_{\text{bottom}}} \tag{2.5}$$

where

$$T_s = \text{ambient temperature}$$
$$h = \text{surface convection constant.}$$

For our model we can assume $T_s = 0$ and compute the change in temperature with respect to ambient temperature.

It is convenient to define the dimensionless parameter Bi called the Biot number. The Bi number is a measure of efficiency of the heat transport across the boundary with regard to internal heat conductance. It is defined by

$$Bi = \frac{hl}{K}.$$

For small values of the Biot number, the test apparatus is weakly coupled to the ambient temperature outside the glass. For large values of the Biot number, there is a strong coupling to the ambient temperature and the surface tends to approach this outside temperature.

2.2.5 Characteristic Scaling.

Certain characteristic scaling was introduced to convert the variables into dimensionless variables. This allows our calculations to be unit free or independent of particular units chosen. In other words, the physical law (i.e. the heat equation) remains valid regardless of the units chosen to express the variables [6]. "The solutions

of problems in conduction of heat can always be expressed in terms of a number of dimensionless quantities" [9]. The dimensionless variables are defined in the following manner:

$$r = l\upsilon, \qquad z = l\zeta, \qquad t = \frac{l^2\tau}{\kappa},$$

$$T = uT_0, \qquad \text{and} \qquad T_0 = \frac{Sl^2}{K}$$

where

$$\begin{aligned} l &= \text{length} \\ \upsilon &= \text{dimensionless length} \\ \zeta &= \text{dimensionless thickness} \\ \tau &= \text{dimensionless time} \\ u &= \text{dimensionless temperature} \\ T_0 &= \text{initial temperature.} \end{aligned}$$

Before proceeding with the numerical evaluation that utilizes these characteristic scales, the assumptions formulated for the thermal model will be discussed.

2.2.6 Assumptions.

Due to constraints involved with modeling a laboratory experiment, certain assumptions were made during development of the numerical model. The assumptions are summarized below.

- The source term is uniform and is considered to be either on or off.
- The carbon black absorbs all optical energy and converts it to thermal energy.
- The glass absorbs/radiates none of the thermal energy.
- The carbon black region has the same thermal properties as the glass slides.
- Certain characteristic or dimensionless scales are used in the model.

In addition, one parameter of the laboratory experiment described above was altered after completion of this research's thermal model. The current width of the coverslip wells is 50 μm which was increased from 3 μm. The depth of the wells was also increased from 1 μm to a varying 3 to 5 μm. This expanded well size and subsequent population of the wells with spores allowed air to be trapped within the wells. The addition of air in between the spores and the soda lime glass is significant because only the glass properties were considered in the original thermal diffusion model, and heat dissipates through glass and air at a different rate. But diffusivity, κ, for soda lime glass is 0.438×10^{-2} cm^2/sec while $\kappa = 0.2216\,$cm^2/sec for air so the ratio of diffusivity ($\kappa_{\text{air}}/\kappa_{\text{glass}}$) is 50.559. This implies that the rate of heat propagation through the test apparatus with the addition of the air pocket, is much smaller than the rate of the original model. Since we are primarily concerned with the thermal effect on the adjacent spore well and the original model overestimates this measurement, this parameter was not altered. These assumptions and the characteristic scales were used to develop and implement the dimensionless numerically evaluated model.

2.2.7 Numerical Methods.

By utilizing characteristic scaling, the axisymmetric, two-dimensional thermal diffusion system of equations (Equations (2.2), (2.3), (2.4), and (2.5)) becomes

$$\frac{\partial u}{\partial t} = \frac{\partial^2 u}{\partial r^2} + \frac{1}{r}\frac{\partial u}{\partial r} + \frac{\partial^2 u}{\partial z^2} + s \tag{2.6}$$

$$\frac{\partial u}{\partial r}(0, z, t) = 0 \tag{2.7}$$

$$\frac{\partial u}{\partial z}(r, z_{\text{top}}, t) = -Bi\, u \tag{2.8}$$

$$\frac{\partial u}{\partial z}(r, z_{\text{bottom}}, t) = Bi\, u \tag{2.9}$$

$$u(r, z, 0) = 0 \tag{2.10}$$

where t is time, r is the radius, z is the distance through the thickness of the test apparatus, and s is the dimensionless source.

This system of equations is numerically evaluated via a second-order Crank-Nicolson finite-difference scheme with Strang splitting. A second-order method implies the truncation error propagated by the Crank-Nicolson scheme is on the order of $(\Delta t)^2$ where Δt is the time step chosen for the model. More importantly, the Crank-Nicolson method has many stability advantages. It is an implicit method and it is absolutely stable which implies that for a stable differential equation and step size, any perturbation created in one time step is not amplified in subsequent time steps.

Before numerically discretizing this equation, we implement Strang splitting by splitting the $\frac{\partial}{\partial t}$ operator into its dimensional components and apply half of the source to each dimension. Thus, Equation (2.6) is converted into

$$\frac{\partial u^*}{\partial t} = \frac{\partial^2 u}{\partial r^2} + \frac{1}{r}\frac{\partial u}{\partial r} + \tfrac{1}{2}s \tag{2.11}$$

$$\frac{\partial u}{\partial t} = \frac{\partial^2 u^*}{\partial z^2} + \tfrac{1}{2}s. \tag{2.12}$$

Strang splitting is applied in order to maintain the second order error caused by splitting the operator in time. It is implemented by solving Equation (2.11) for half of a time step, then solving Equation (2.12) for a full time step, and finally solving Equation (2.11) for another half time step [25].

Let U be the numerical approximation to u, specifically

$$U_{j,k}^n = u\left(r_j, z_k, t_n\right)$$

where

$$r_j = (j-1)\Delta r, \qquad z_k = k\Delta z, \qquad \text{and} \qquad t_n = n\Delta t$$

and Δr is the spatial step in the radial direction and Δz is the spatial step in the z direction (thickness) while n, j, and k are the number of iterations such that $1 < j < N$ and $1 < k < N$. Through use of the Crank-Nicolson discretization with respect to

space and time, Equation (2.11) becomes

$$U_{j,k}^{n+1} - U_{j,k}^{n} = \frac{\Delta t}{2\Delta r^2}\left[\left(U_{j+1,k}^{n+1} - 2U_{j,k}^{n+1} + U_{j-1,k}^{n+1}\right) + \left(U_{j+1,k}^{n} - 2U_{j,k}^{n} + U_{j-1,k}^{n}\right)\right] + \frac{\Delta t}{4r_j\Delta r}\left[\left(U_{j+1,k}^{n+1} - U_{j-1,k}^{n+1}\right) + \left(U_{j+1,k}^{n} - U_{j-1,k}^{n}\right)\right] + \frac{\Delta t}{2}s \tag{2.13}$$

Similarly, Equation (2.12) leads to

$$U_{j,k}^{n+1} - U_{j,k}^{n} = \frac{\Delta t}{2\Delta z^2}\left[\left(U_{j,k+1}^{n+1} - 2U_{j,k}^{n+1} + U_{j,k-1}^{n+1}\right) + \left(U_{j,k+1}^{n} - 2U_{j,k}^{n} + U_{j,k-1}^{n}\right)\right] + \frac{\Delta t}{2}s \tag{2.14}$$

Our model has a uniform mesh or equal grid spacing in both the radial and thickness directions, that is, $\Delta r = \Delta z$.

Along the left-hand boundary of the model area (where $r = 0$), the cylindrical heat equation becomes invalid due to the $\frac{1}{r}\frac{\partial u}{\partial r}$ term in Equation (2.11). This issue is resolved by treating t as a constant and expanding U around $r = 0$ via Taylor series expansion. By means of this method, a centered-difference approximation can be obtained and Equation (2.7) becomes

$$U_{1,k}^{n+1} - U_{1,k}^{n} = \frac{2\Delta t}{(\Delta r)^2}\left[(U_{2,k}^{n+1} - U_{1,k}^{n+1}) + (U_{2,k}^{n} - U_{1,k}^{n})\right] \tag{2.15}$$

where $j = 1$ is the left-hand boundary [31]. Equation (2.15) is applied within the model at the center of the left side of the domain (where $r = 0$). Near the right side of the model area we will be measuring the effect of the thermal heating as it propagates toward the adjacent spore well. Dirichlet boundary conditions are implemented at the right-hand domain far enough from our sampling that it does not impact the solution.

The boundary conditions along the top and bottom of the slides are also found by means of a difference approximation. Equations (2.8) and (2.9) give

$$U_{j,N}^{n+1} - U_{j,N}^{n} = Bi_{\text{top}}^{*} \Delta t \left(U_{j,N}^{n+1} - U_{j,N}^{n+1} \right) \tag{2.16}$$

$$U_{j,1}^{n+1} - U_{j,1}^{n} = Bi_{\text{bottom}}^{*} \Delta t \left(U_{j,1}^{n+1} - U_{j,1}^{n} \right) \tag{2.17}$$

where

$$Bi_{\text{top}}^{*} = \frac{-Bi}{2 + Bi\Delta z^2} \qquad \text{and} \qquad Bi_{\text{bottom}}^{*} = \frac{Bi}{2 - Bi\Delta z^2}.$$

The top boundary of the slides is defined to be $k = N$ while $k = 1$ is the bottom boundary. Equations (2.16) and (2.17) are applied within the model at the top and bottom of the domain. The thermal model consisting of Equations (2.13), (2.14), (2.15), (2.16), and (2.17) was implemented and numerically evaluated in MATLAB in order to determine the effects of thermal diffusion throughout the spores and the test apparatus. For details of the MATLAB code, refer to Appendix A.

2.3 Results

As discussed in Section 2.2.1, our model is concerned with two main measurements. The first is a comparison of the temperature that the spores are experiencing as opposed to the temperature that the carbon black is encountering. These results are illustrated in Figure 2.5. The top line is the dimensionless temperature calculated at the center of the source (the carbon black well). The bottom line represents the dimensionless temperature that the spores directly beneath the center of the source are subjected to. The spore temperature is calculated 4 μm below the carbon black which corresponds to the average depth of the spore wells. The x-axis represents time and clearly shown in the plot is a 0.12 second application of the thermal source. The 0.12 second exposure reflects the fastest raster rate utilized within the laboratory experiment. The y-axis is dimensionless temperature, or to be more exact, it is the percentage temperature change from ambient temperature. By comparing the respective dimensionless temperatures at 0.12 seconds, the spores were found to experience

approximately 93.1% of the heat that the carbon black emitted. Also of note is the time it takes for the temperatures of the spores and carbon black to ramp up to a steady state value. Both the spores and the carbon black reach approximately 92% of their total dimensionless temperature within 0.014 seconds. They reach 85% at approximately 6.85×10^{-3} seconds. These measurements were calculated with a heat transfer coefficient of $h = 2 \times 10^{-3}\,\mathrm{W/cm^2\,^\circ C}$ which led to $Bi = .0213$ [43].

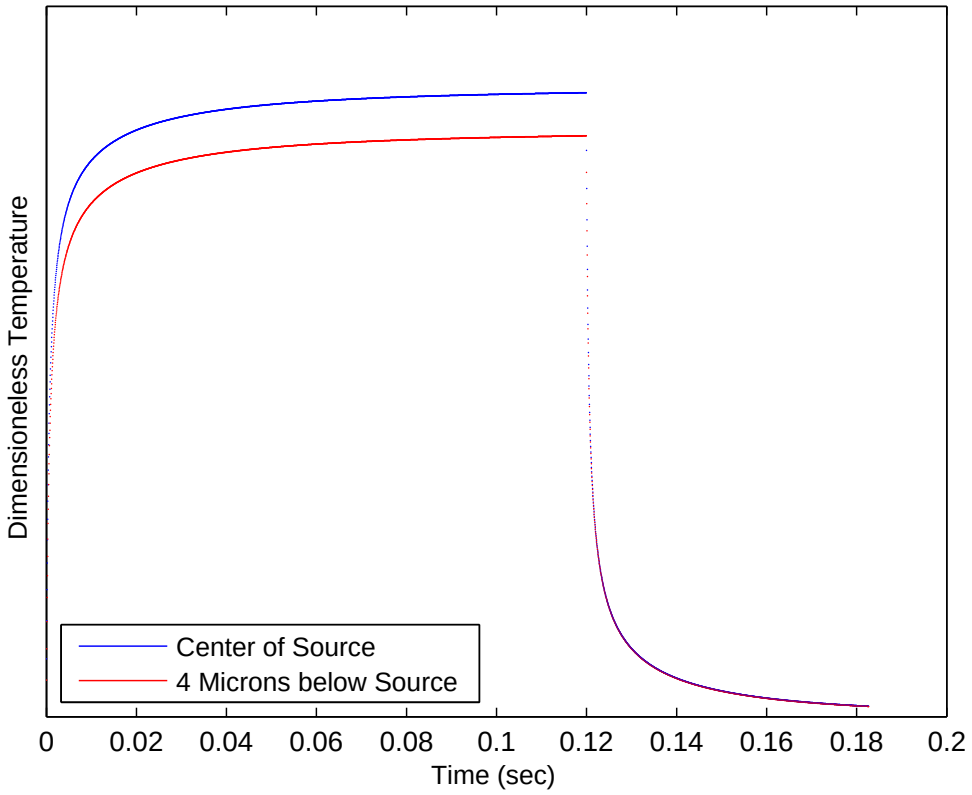

Figure 2.5: Source and Spore Temperature Profile for 0.12 Second Exposure

The second parameter of interest within the model is the temperature effect felt by the adjacent spore. Figure 2.6 illustrates the dimensionless temperature profile at the point halfway in between spore wells (refer to Figure 2.3). This characterization was also calculated for a 0.12 second application of the source. It takes approximately 0.05 seconds for any heat to dissipate from the carbon black well to the point of interest. The max temperature is realized at approximately 0.18 seconds which is

0.06 seconds after the source is turned off. Most significant is that the temperature experienced at this point is on the order of 10^{-4} less compared to the maximum temperature experienced at the center of the carbon black. Therefore, since this profile is taken halfway in between adjacent source wells, the effect of a carbon black well on the adjacent spore is negligible.

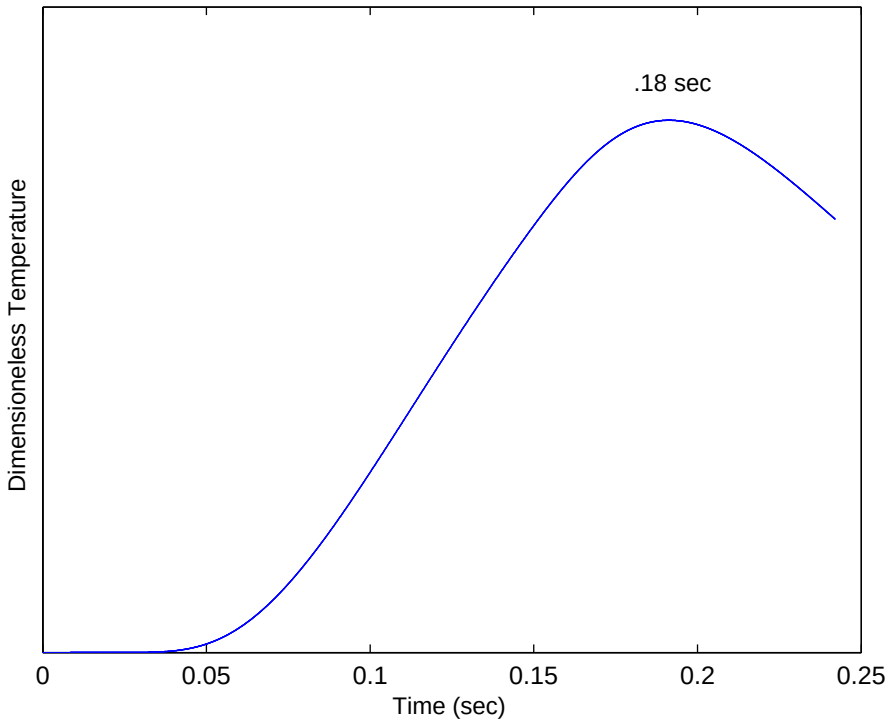

Figure 2.6: Temperature Profile Halfway Between Adjacent Carbon Black Wells

2.4 Conclusion

The thermal model developed in this chapter produces two main results. The change in temperature experienced by the spores is approximately 93.1% of the temperature change seen by the carbon black. This measurement allows a more accurate development of a probability of kill model for the thermal heating method designed in the laboratory experiment. More important is the depiction of the temperature profile halfway between adjacent carbon black wells. The negligible effect of one carbon

black well on the adjacent spore is also necessary to develop an accurate probability of kill model. In addition, this calculation allows modification of future experiments in order to ease the challenges that the 1500 μm separation of carbon black wells created within the laboratory. The characterization of thermal heating of a spore raises the question of exactly how the spore is being damaged. The next two chapters describe our proposal of the events occurring within a spore that causes the spore to be damaged to such an extent that the spore is effectively dead.

III. Diffusion Model

3.1 Introduction

Now that our method of thermal exposure is understood, we will examine the effects of the thermal damage on the spore itself. By applying heat to a spore, we energize adsorbed, absorbed, and chemically bound water molecules. Adsorbed water molecules are bound to the outside surface of a spore and they become mobile when heated to temperatures between approximately 100 to 120 °C. Absorbed and chemically bound water molecules are found within the spore. Absorbed molecules become available at temperatures similar to adsorbed water while chemically bound water molecules become available only at temperatures above approximately 300 °C. These measurements are consistent with thermo-gravimetric analysis studies which confirm significant weight losses of *Bacillus* spores when heated to temperatures of 100 °C and 300 °C [22]. Some chemically bound water molecules are released through Maillard reactions. Maillard reactions are chemical reactions between sugars and proteins that are initiated by heat. Maillard reactions occur within different phases but two of these phases cause water molecules to break away from proteins or amino acids.

We propose energizing of water molecules allows them to become free water molecules which causes the molecules to be more active in hydrolysis reactions with DNA and proteins, and permits mobility or diffusion of the water within the spore. In addition, diffusion of water between the spore and the environment surrounding it also occurs. This interaction between the spore's outside environment is related to the water concentration of the environment. For example, during dry heating the water concentration of the air surrounding the spore would depend on the ambient humidity. During a wet heating process, the water concentration of the surrounding liquid would effect the diffusion of water in and out of the spore. The release and mobility of water leads to hydrolysis reactions within the spore which will be discussed

in further detail within Chapter IV. In order to accomplish this, we must first have an appreciation of the structure of a spore.

3.2 Structure of Bacillus Spores

Bacillus spores are constructed of concentric layers all of which have different roles in regards to the spore's heat resistance. The layers of a *Bacillus* spore are illustrated in Figure 3.1 (layers not drawn to scale). We will discuss each layer in detail.

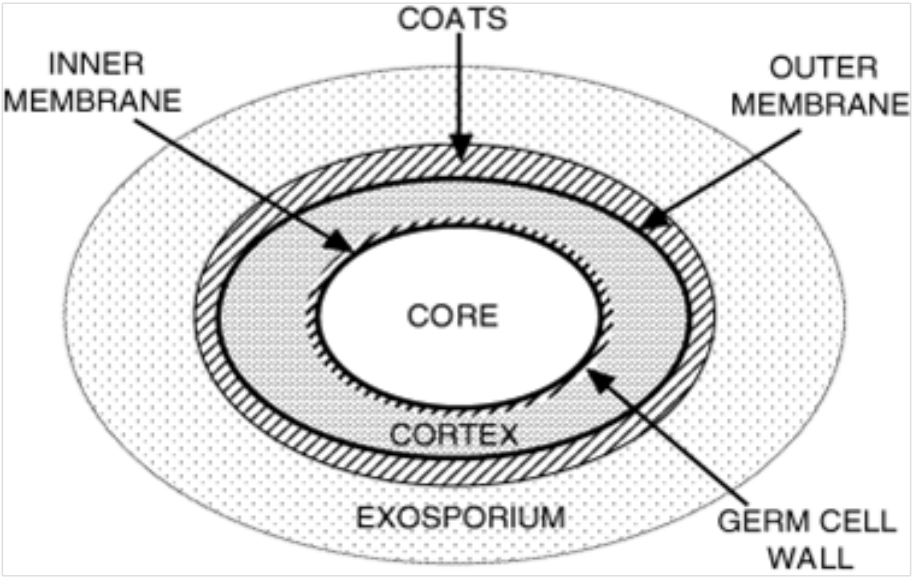

Figure 3.1: Structure of Spore [40]

The outermost layer is the exosporium and as already stated, the exosporium is not present on all species of the *Bacillus* genus. Most importantly, the exosporium is not believed to provide extra protection or heat resistance [21]. The exosporium is mostly made up of proteins.

Inside the exosporium lies the spore coat which is composed of several layers. It is also made up of proteins. It has been shown that heat resistance does not depend on the spore coat [16]. Immediately inside the spore coat lies the outer membrane. Although the exact function of the outer membrane is not understood,

the outer membrane "has no notable effect of spore resistance to heat" [40]. In addition, it is not thought to be a significant permeability barrier. Westphal and others found that an increase in relative humidity caused a spore to swell due to water intake [46]. Therefore, we will assume that the exosporium, the spore coat, and the outer membrane are all permeable with respect to water molecules.

The next layer of a spore is the cortex, which is made up of peptidoglycan. The cortex reduces the water content of the spore core by allowing small molecules, like water, to pass through. Similarly, the cortex keeps DNA, which lies in the core, dry. The germ cell wall which is also made up of peptidoglycan becomes the cell wall of the outgrowing spore once germination occurs. The germ cell wall provide no heat resistance for the spore [20, 40].

The inner membrane separates the core from the cortex and it is believed that the inner membrane provides a strong permeability barrier to protect the core from any damage. However, Xu, Labuza, and Diez-Gonzalez heated *B.a.* spores within sodium hypochlorite and found that this caused the leakage of dipicolinic acid (DPA). Since DPA is contained within the core, this study proved one method of increasing the inner membrane's permeability [47]. Another study by Coleman, Chen, Li, Cowan, and Setlow demonstrated a release of DPA during a moist-heat treatment which "suggested that the permeability barriers that block movement of small molecules in and out of the spore core had been breached" [11]. Therefore, this research assumes a certain permeability of the inner membrane as the spore membranes are damaged.

The innermost layer of a spore is the core. The core contains the DNA, ribosomes, most spore enzymes, and certain proteins. Depending on the species, water makes up 27 to 55% of the core wet weight. In addition, the amount of free water is extremely low which indicates that molecular mobility within the core is almost nonexistent. The core water content is the major contributor to a spore's resistance to wet heat. A spore is more resistant to wet heat with a low core water content [19]. Also significant is the fact that core water content is dependent upon sporulation, or

reproduction, temperatures and spore preparation temperatures. Core water content has an inverse relationship with preparation temperatures, the higher the preparation temperature, the lower the core water content [28]. Due to an understanding of a spore's structure and the varying roles in relation to heat resistance, we can now develop a model to illustrate mobility of water within a spore.

3.3 Reaction Kinetics

Before proceeding with the mobility model, it is necessary to discuss chemical reactions that will occur within the spore. These chemical reactions, which are known as reaction kinetics, are governed by rates of reactions. The main factors influencing the reaction rates are the concentration and physical state of the reactants, the temporal behavior of the reactants, and the presence of any catalysts in the reaction [32]. For example, in Section 4.3 we will model the rate of DNA damage by:

$$\frac{\mathrm{d}\,[\mathrm{DNA}]}{\mathrm{d}t} = -k_1\,[\mathrm{DNA}] - k_2\,[\mathrm{H_2O}]\,[\mathrm{DNA}]$$

where

$[\mathrm{DNA}]$ =information content of DNA

k_1 =rate coefficient associated with $[\mathrm{DNA}]$ breakdown during pyrolitic thermal damage

k_2 =rate coefficient associated with $[\mathrm{DNA}]$ breakdown during hydrolysis

$[\mathrm{H_2O}]$ =average water concentration.

The first term represents pyrolysis reactions which damage DNA at high temperatures while the second term represents hydrolysis reactions which damage [DNA] at lower temperatures if water is present. The units of [DNA] and $[\mathrm{H_2O}]$ are given by molality. Molality is denoted by *molal* and defined as the number of moles of solute per kilogram of solvent. In the case of [DNA] it represents the concentration of base pair encoding

information. The concept of reaction kinetics will be used throughout the water mobility and kill probability models.

3.4 Water Mobility Model

The water mobility model will be based on a production/diffusion equation. Molecular diffusion is the movement of molecules from a region of higher concentration to that of a region with a lower concentration. This transport of molecules is founded on random molecular movement. As we are modeling the diffusion throughout a spore, we have a three dimensional volume to consider. Diffusion is mathematically modeled via the multi-dimensional Fick's law which predicts how diffusion affects the concentration of water over time [27]:

$$\frac{\partial w}{\partial t} = f(w) + \nabla \cdot D\nabla w \tag{3.1}$$

where

$$\begin{aligned} w &= \text{concentration of mobile water (molal)} \\ t &= \text{time (sec)} \\ f(w) &= \text{production of water (molal/sec)} \\ D &= \text{diffusion coefficient } (\text{cm}^2/\text{sec}). \end{aligned}$$

The diffusion coefficient is a measure of the mobility of water within the spore. Note that when $f(w)$ is negative, water is being consumed. Similarly, when $f(w)$ is positive, water is produced.

3.4.1 Initial Distribution.

Due to the properties of a spore's structure, there are only two main spore layers to consider when discussing the initial distribution of water throughout a spore. These layers are the core, which contains DNA, and the cortex. As previously stated, the core

contains an extremely low amount of liquid water molecules, or absorbed water. Thus for the purpose of our model, we will consider the concentration of absorbed water in the core to be zero. But taking into account that water makes up a certain percentage of the core wet weight, we must assume chemically bound water exists within the core. The cortex allows mobility of water molecules so it contains absorbed water molecules along with its chemically bound water molecules. Refer to Figure 3.2 for a graphical illustration of a notional distribution of water throughout the spore. As we will be scaling the radius of a spore to one, the radius of the core, r_c, is approximately 75% of the radius of the entire spore, designated by r_o [34,46]. Note that we are assuming an equal amount of chemically bound water throughout the core and cortex while only the cortex contains absorbed water. The distribution of water outside the spore will depend on ambient water concentration, which in turn, depends on whether a wet or dry heating process is utilized.

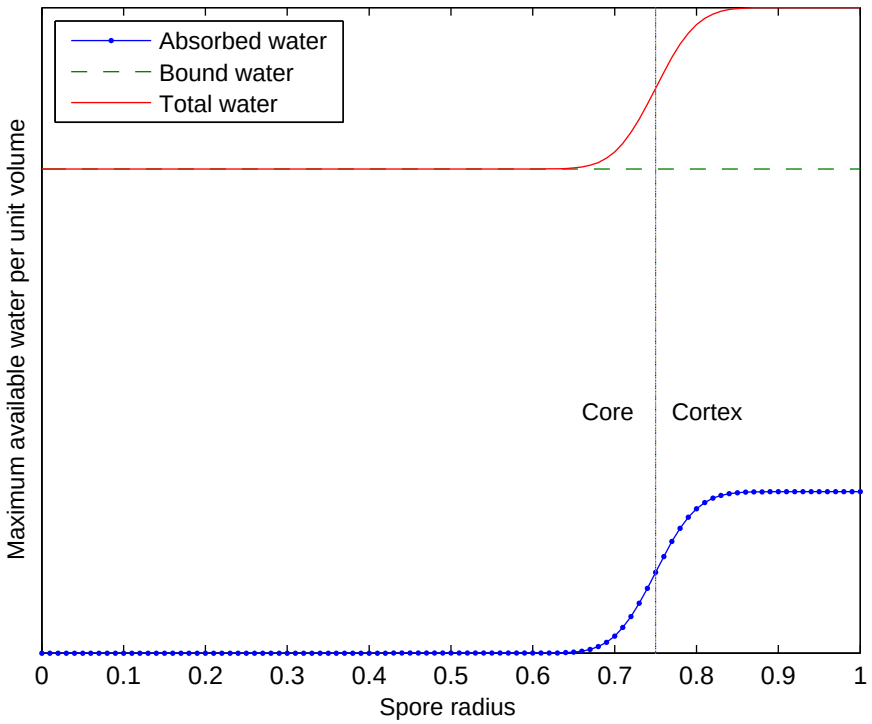

Figure 3.2: Initial Distribution of Water Throughout Radius of Spore

3.4.2 Release of Water.

Now that we have determined the initial distribution of available water throughout the spore, we need to calculate how this absorbed and chemically bound water is released. In other words, how does the water become mobile? We propose that by applying heat to the spore, the absorbed and chemically bound water molecules become energized. Once energized, the water becomes mobile in a free molecular state similar to a gaseous state.

$$[H_2O]_\ell + \text{Heat} \longrightarrow [H_2O]_g$$
$$[H_2O]_b + \text{Heat} \longrightarrow [H_2O]_g$$

where

$[H_2O]_\ell$ = initial concentration of absorbed water molecules (molal)

$[H_2O]_b$ = initial concentration of chemically bound water molecules (molal)

$[H_2O]_g$ = initial concentration of mobile water molecules (molal).

These two sources of mobile water are energized at different temperatures. Absorbed water is released at approximately 100 °C while bound water requires a much higher temperature of approximately 300 °C. We choose to model their respective release functions as a Gaussian density function centered about their respective mean release temperatures T_1 and T_2 with associated standard deviations σ_1 and σ_2, i.e.

$$g_i(T) = \frac{1}{\sigma_i\sqrt{2\pi}} e^{-\left(\frac{T-T_i}{\sqrt{2}\sigma_i}\right)^2} \qquad i = 1, 2.$$

These functions are illustrated in Figure 3.3 using T_1=100 °C, σ_1=20, T_2=300 °C, and σ_2=50. We observe that absorbed water is released in a neighborhood of 100°C until all the absorbed water is active. Then bound water begins its release to a peak of 300 °C. These measurements were chosen to approximate the thermo-gravimetric

analysis results found by Holwitt, Kiel, Alls, Morales, and Gifford [22]. Their study found that approximately 10% of the initial weight of a *Bacillus thuringiensis* spore was lost by 100 °C and 40% was lost by approximately 300 °C.

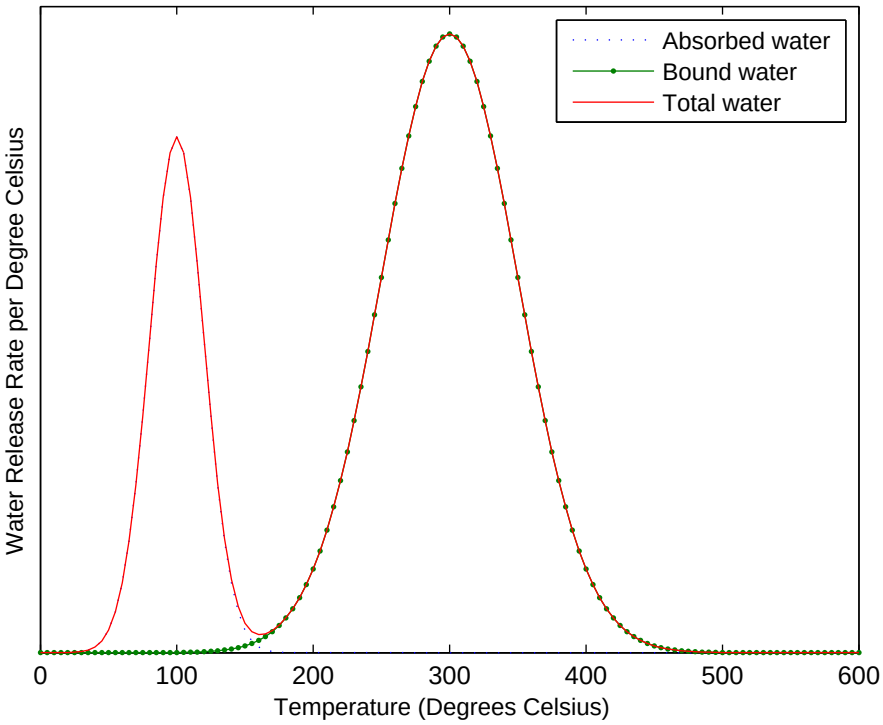

Figure 3.3: Distribution of Water Released at 100 and 300°C

The total mobile water released at any given temperature, T^*, is determined by integrating the weighted sum of these Gaussian functions i.e.

$$\begin{aligned}[\mathrm{H_2O}]_g &= \int_{-\infty}^{T_*} [\mathrm{H_2O}]_\ell \, g_1(\tau) + [\mathrm{H_2O}]_b \, g_2(\tau) \mathrm{d}\tau \\ &= [\mathrm{H_2O}]_\ell \, f_1(T^*) + [\mathrm{H_2O}]_b \, f_2(T^*) \end{aligned} \tag{3.2}$$

where

$$f_i(T^*) = \tfrac{1}{2}\left[1 + \mathrm{erf}\left(\frac{T^* - T_i}{\sqrt{2}\sigma_i}\right)\right] \qquad i = 1, 2 \tag{3.3}$$

and erf is the error function [1]. We will assume that given a particular T^*, this temperature is reached instantaneously and therefore the initial amount of released

water in the spore is dependent on T^*. This is consistent with Chapter II results that illustrated the immediate increase in temperature once the heat source was applied (refer to Figure 2.5).

Figure 3.4 shows the results of this integration using the values from Figure 3.3, $[H_2O]_\ell$=1, and $[H_2O]_b$=3. This figure illustrates the effect on the available mobile water as temperatures increase through the release temperature for absorbed water to the release temperature for bound water.

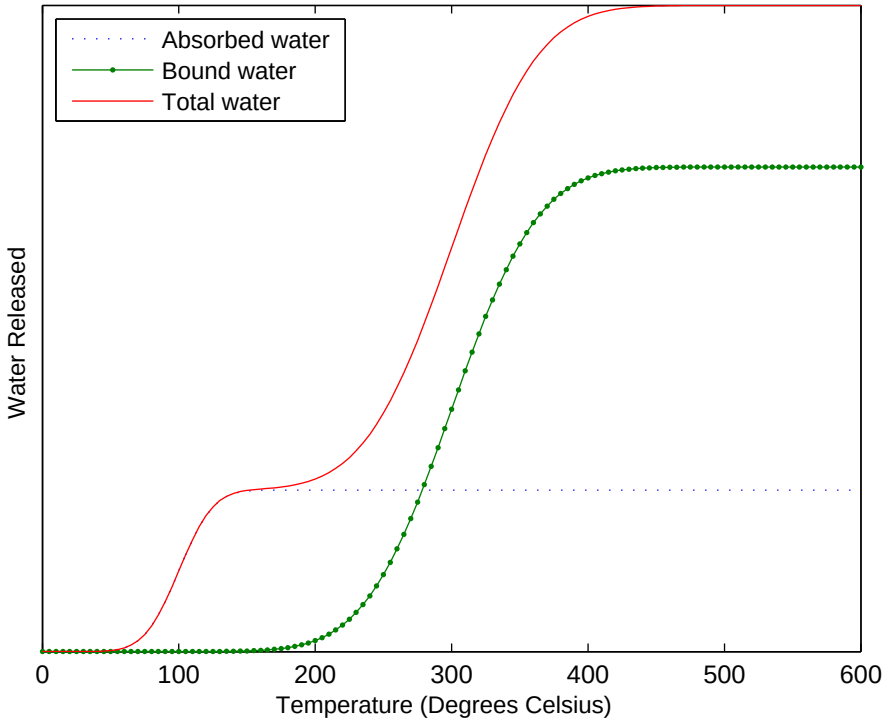

Figure 3.4: Total Water Released as Temperature Increases

This function serves as our initial distribution of mobile water in the spore for the water mobility model. That is,

$$w(r,0) = [H_2O]_g(r) \tag{3.4}$$

where r is the radius.

3.4.3 Analytical Analysis.

3.4.3.1 Production Term.

Water is consumed through reaction with hydrocarbon compounds within the spore such as DNA and proteins, thus the production term in Equation (3.1) is reduced to a simple first order reaction term:

$$f(w) = -k_t w \tag{3.5}$$

where k_t is the total reaction rate constant. It is effectively the averaged rate for all possible hydrolysis reactions in the spore. The value k_t follows the Arrhenius equation which models the rate of chemical reactions [27]:

$$k_t(T) = A\mathrm{e}^{-\frac{E}{RT}}$$

where

$$A = \text{encounter frequency}$$
$$E = \text{activation energy}$$
$$R = \text{gas constant.}$$

3.4.3.2 Boundary Conditions.

For the purpose of this analysis, we assume a spore is a symmetric sphere. We model the diffusion of water radially from the spore's core into the cortex and the surrounding environment. At the boundary where the radius is equal to zero, the solution must be finite, that is,

$$|w(0,t)| < \infty. \tag{3.6}$$

Where the radius is equal to the total spore radius ($r = r_o$), the boundary condition follows a similar argument to the Newton's law of cooling boundary condition found in Section 2.2.4 of the thermal model. In other words, the flow of water across the outside boundary is proportional to the water content in the spore at the outer boundary and the ambient humidity. The boundary condition is modeled by,

$$-\hat{n} \cdot D\nabla w\left(r_o, t\right) = h\left\{w\left(r_o, t\right) - \left[H_2O\right]_a\right\} \tag{3.7}$$

where

$$\begin{aligned} \hat{n} &= \text{outward normal vector} \\ \left[H_2O\right]_a &= \text{water concentration outside spore (molal)} \\ h &= \text{surface flow velocity.} \end{aligned}$$

Note that we are assuming the external $\left[H_2O\right]_a$ vapor is at the spore temperature T^*. Also for spherical geometry, $\hat{n}$ becomes the outward radial direction. Therefore, Equation (3.7) becomes

$$-D\frac{\partial w}{\partial r}\left(r_o, t\right) = h\left\{w\left(r_o, t\right) - \left[\mathrm{H_2O}\right]_a\right\}. \tag{3.8}$$

The combination of Equations (3.1), (3.2), (3.3), (3.4), (3.5), (3.6), and (3.8) constitute the water mobility model.

3.4.3.3 Analytical Solution.

We assume the spore is spherically symmetric, that is, it has no angular dependence. This allows the model to become one dimensional with respect to the radius of the spore and time ($w(r,t)$). Further, we shall assume the diffusivity, D, remains constant across the radius of the spore. Thus, the diffusion term in Equation (3.1)

becomes

$$\nabla \cdot D\nabla w = D\left(\frac{\partial^2 w}{\partial r^2} + \frac{2}{r}\frac{\partial w}{\partial r}\right). \tag{3.9}$$

At this point we introduce dimensionless variables by choosing characteristic scales for length, time, and water concentration. To this end, we scale all lengths by the radius of the spore r_o, time by the diffusion time $t_c = r_o^2/D$, and water concentration by the maximum concentration of initial released water $[\mathrm{H_2O}]_M$, i.e.

$$[\mathrm{H_2O}]_M = \max_{0<r<r_o} [\mathrm{H_2O}]_g (r, T^*).$$

We will assume in this model, that $[\mathrm{H_2O}]_a$ and $[\mathrm{H_2O}]_b$ are constants and define dimensionless variables x, τ, and v by

$$r = r_o x, \qquad t = t_c \tau, \qquad w(r,t) = [\mathrm{H_2O}]_M \, v(x,\tau). \tag{3.10}$$

Substituting these variables into Equations (3.1), (3.2), (3.6), and (3.8) leads to

$$\frac{\partial v}{\partial \tau} = -\beta v + \frac{1}{x^2}\frac{\partial}{\partial x}\left(x^2 \frac{\partial v}{\partial x}\right) \qquad 0 < x < 1,\ \tau > 0 \tag{3.11}$$

$$\frac{\partial v}{\partial x}(0,\tau) = 0 \qquad \tau > 0 \tag{3.12}$$

$$-\frac{\partial v}{\partial x}(1,\tau) = B(v(1,\tau) - \gamma) \qquad \tau > 0 \tag{3.13}$$

$$v(x,0) = \alpha_1(x) f_1(T^*) + \alpha_2(x) f_2(T^*) \qquad 0 < x < 1 \tag{3.14}$$

where

$$B = \frac{r_o h}{D}, \qquad \beta = \frac{r_o^2 k_t}{D}, \qquad \text{and} \qquad \gamma = \frac{[\mathrm{H_2O}]_a}{[\mathrm{H_2O}]_M}$$

with

$$\alpha_1(x) = \frac{[\mathrm{H_2O}]_\ell}{[\mathrm{H_2O}]_M}(r_o x) \qquad \text{and} \qquad \alpha_2(x) = \frac{[\mathrm{H_2O}]_b}{[\mathrm{H_2O}]_M}(r_o x).$$

These parameters have important physical interpretations. First, we observe that γ is the ratio of the water concentration at the boundary of the spore to that

within the spore. For wet heating we would expect γ to be greater than one while for dry heating this parameter would be less than one. Next, we examine B and β as the ratio of time scales. There are three time scales which naturally present themselves in this water diffusion model. They are the diffusion time, t_D, the hydrolysis reaction time, t_R, and the surface convection time, t_S. They can be defined as follows:

$$t_D = \frac{r_0^2}{D}, \qquad t_R = \frac{1}{k_t}, \qquad \text{and} \qquad t_S = \frac{r_0}{h}$$

recalling that k_t is the total reaction rate constant. These times can be ordered from smallest to largest, for example $t_R < t_D < t_S$. This ordering suggests the priority at which these processes take place. So for the above ordering, hydrolysis reactions occur much faster than diffusion through the spore or convection away from the spore surface. Further, by definition we see

$$B = \frac{t_D}{t_S} < 1 \qquad \text{and} \qquad \beta = \frac{t_D}{t_R} > 1$$

with this ordering. Because diffusivity, D, surface convection, h, and the reaction coefficient, k_t, are temperature dependent, this time scale ordering may change with temperature and influence the mobile water concentration found in hydrolysis reactions.

Using separation of variables, the homogeneous problem given by Equation (3.11) and the homogeneous boundary conditions becomes

$$h'(\tau) + (\beta + \mu)h(\tau) = 0 \tag{3.15}$$

$$\left[x^2 g'(x)\right]' + \mu x^2 g(x) = 0 \tag{3.16}$$

$$g'(0) = 0 \tag{3.17}$$

$$-g'(1) = B\, g(1) \tag{3.18}$$

where μ is a separation parameter. The eigenvalues and eigenfunctions are found by solving Equations (3.16), (3.17), and (3.18) with respect to the homogeneous bound-

ary conditions. The associated eigenfunctions are of the form

$$g_n(x) = K_n \frac{\sin(s_n x)}{x}, \qquad n \in \mathbb{N}$$

where

$$K_n = \sqrt{\frac{2(1-B)}{\sin^2(s_n) - B}}$$

is found by normalizing g_n and s_n satisfies the transcendental equation

$$\tan(s_n) = \frac{s_n}{1-B}.$$

Notice these eigenfunctions could also be represented in terms of spherical Bessel functions as [1]

$$g_n(x) = K_n s_n j_0(s_n x).$$

These eigenfunctions are orthonormal with respect to the weight x^2, i.e.

$$\langle g_n, g_m \rangle = \int_0^1 x^2 g_n(x) g_m(x) \mathrm{d}x = \delta_{mn}.$$

Now we seek a solution to the homogeneous system of the form

$$v(x,\tau) = \gamma + \sum_{n=1}^{\infty} h_n(\tau) g_n(x). \tag{3.19}$$

Introducing Equation (3.19) back into Equation (3.11) gives

$$h_n'(\tau) + \omega_n h_n(\tau) = -\beta\gamma \langle 1, g_n \rangle \tag{3.20}$$

where

$$\omega_n = \beta + s_n^2.$$

Equation (3.20) along with the initial conditions (Equation (3.14)) produces the solution to the first-order differential equation:

$$h_n(\tau) = F_n(T^*)\mathrm{e}^{-\omega_n\tau} - \frac{\gamma\langle 1, g_n\rangle}{\omega_n}\left[\beta + s_n^2\mathrm{e}^{-\omega_n\tau}\right] \tag{3.21}$$

where $F_n(T^*) = f_1(T^*)\langle\alpha_1, g_n\rangle + f_2(T^*)\langle\alpha_2, g_n\rangle$.

Inserting Equation (3.21) into Equation (3.19) and reducing terms gives

$$v(x,\tau) = \sum_{n=1}^{\infty} F_n(T^*)\mathrm{e}^{-\omega_n\tau}g_n(x) + \gamma\sum_{n=1}^{\infty}\langle 1, g_n\rangle\frac{s_n^2}{\omega_n}\left[1 - \mathrm{e}^{-\omega_n\tau}\right]g_n(x). \tag{3.22}$$

The first series represents the influence of the initial water distribution while the second series represents the influence of the wet or dry heating (denoted by γ). Recall from Equation (3.10) that

$$w(r,t) = [\mathrm{H_2O}]_M\, v(x,\tau). \tag{3.23}$$

DNA is only present in the spore core. Thus all the hydrolysis reactions with DNA will occur in the core so we are only concerned with the diffusion of water within the spore core. The average total mobile water concentration in the core is given by

$$[\mathrm{H_2O}]_c(t) = \frac{3}{r_c^3}\int_0^{r_c} w(r,t)r^2\mathrm{d}r. \tag{3.24}$$

Equation (3.24) with the inclusion of the dimensionless variables and Equation (3.22), reduces to

$$[\mathrm{H_2O}]_c(t_c\tau) = \frac{3}{x_c^3}[\mathrm{H_2O}]_M\left\{\sum_{n=1}^{\infty}F_n(T^*)G_n(x_c)\mathrm{e}^{-\omega_n\tau} + \gamma\sum_{n=1}^{\infty}G_n(1)G_n(x_c)\frac{s_n^2}{\omega_n}\left[1-\mathrm{e}^{-\omega_n\tau}\right]\right\} \tag{3.25}$$

where x_c is defined as r_c/r_o and

$$G_n(x) = \int_0^x \xi^2 g_n(\xi) \mathrm{d}\xi. \tag{3.26}$$

Notice if $x = 1$ then Equation (3.26) gives

$$G_n(1) = \int_0^1 x^2 g_n(x) \mathrm{d}x = \langle 1, g_n \rangle .$$

Equation (3.25) contains important limiting behaviors. For short time periods (small values of t), the second term approaches zero implying that the first term, or the influence of local water, dictates the release, diffusion, and reaction of water in the core. Only during longer time periods does the effect of the water concentration outside the spore become relevant. For more details of the analytical solution, see Appendix B.

3.4.3.4 Steady State Solution.

The steady state solution is obtained from Equation (3.11) where $\frac{\partial v}{\partial \tau}$ is assumed to vanish. Along with the boundary conditions (Equations (3.12) and (3.13)), the steady state problem becomes

$$\begin{aligned} \frac{\mathrm{d}}{\mathrm{d}x}\left(x^2 \frac{\mathrm{d}v_s}{\mathrm{d}x}\right) - \beta x^2 v_s &= 0 \\ \frac{\mathrm{d}v_s}{\mathrm{d}x}(0) &= 0 \\ -\frac{\mathrm{d}v_s}{\mathrm{d}x}(1) &= B(v_s(1) - \gamma) \end{aligned}$$

where s indicates steady state. This boundary value problem admits a solution

$$v_s(x) = \frac{A}{x} \sinh(\sqrt{\beta} x)$$

where

$$A = \frac{\gamma B}{\sqrt{\beta}\cosh(\sqrt{\beta}) - (1-B)\sinh(\sqrt{\beta})}.$$

We are assuming that the environment cannot be perfectly dry thus $\gamma \neq 0$. Now using Equations (3.23) and (3.24), the steady state core water concentration becomes

$$[H_2O]_{sc} = \frac{3}{x_c^3}[H_2O]_M v_{sc} \tag{3.27}$$

with

$$v_{sc} = \frac{\gamma B}{\beta}\left[\frac{\sqrt{\beta}x_c\cosh(\sqrt{\beta}x_c) - \sinh(\sqrt{\beta}x_c)}{\sqrt{\beta}\cosh(\sqrt{\beta}) - (1-B)\sinh(\sqrt{\beta})}\right]. \tag{3.28}$$

The steady state solution represents the limiting behavior of the time dependent core water concentration given in Equation (3.25). In fact, Equation (3.25) can be written as

$$[H_2O]_c(t_c\tau) = [H_2O]_{sc} + \frac{3}{x_c^3}[H_2O]_M \sum_{n=1}^{\infty} C_n e^{-\omega_n \tau}$$

where

$$C_n = \left[F_n(T^*) - \gamma G_n(1)\frac{s_n^2}{\omega_n}\right] G_n(x_c).$$

Steady state is reached at approximately half the diffusion time ($t_s \approx \frac{1}{2}t_D$).

3.5 Water Mobility Model Results

3.5.1 Assumptions.

During development of the water diffusion model which examines water release, diffusion, and reaction within the spore core, the following assumptions were made:

- The geometry of the spore and its properties are spherically symmetric.
- The initial distribution of water depends on adsorbed, absorbed, and chemically bound water molecules outside and throughout the spore.
- These water molecules become gaseous water molecules once released by heating the spores to a certain temperatures.

- The desired temperature, T^*, which is reached instantaneously.
- Diffusion can only take place with gaseous water molecules.
- The gaseous water molecules are consumed in chemical reactions with other molecules such as DNA and proteins (hydrolysis).

In addition to these assumptions, the parameters found in Table 3.1 were used to solve the production/diffusion model [8, 14, 30, 33, 48].

Table 3.1: Water Mobility Model Parameters

Parameter	Value	Units
R	1.986×10^{-3}	kcal/mol°K
D	2.0×10^{-9}	cm^2/sec
h	1.023×10^{3}	cm/sec
A	1.6×10^{3}	sec^{-1}
E	10	kcal/mol
$[H_2O]_M$	25.944	molal

3.5.2 Analytical Results.

Utilizing the assumptions and parameters described above, the model was solved analytically to evaluate the influence that time, temperature, and heating process (wet versus dry) had on the spore core water content. Figure 3.5 was analyzed for $\gamma = 1$ at a temperature of 110 °C. This γ value indicates that the water concentration outside the spore was equivalent to the initial released gaseous water concentration inside the spore. The time behavior of the core water concentration is indicated by the solid line while the steady state result (refer to Equations (3.27) and (3.28)) is given by the dashed line. As previously discussed, over time the core water level will rise as water is released and will equilibrate according to its relationship with the water concentration outside the spore. Using the values in Table 3.1, the diffusion time, t_D, is 1.25 seconds and steady state is reached in approximately 0.6 seconds.

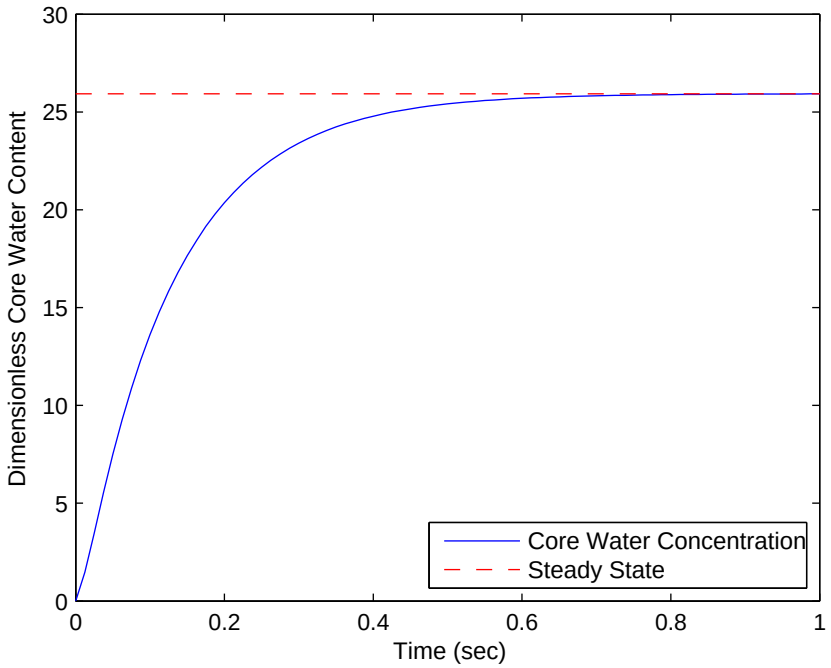

Figure 3.5: Core Water Concentration for γ=1 at 110 °C

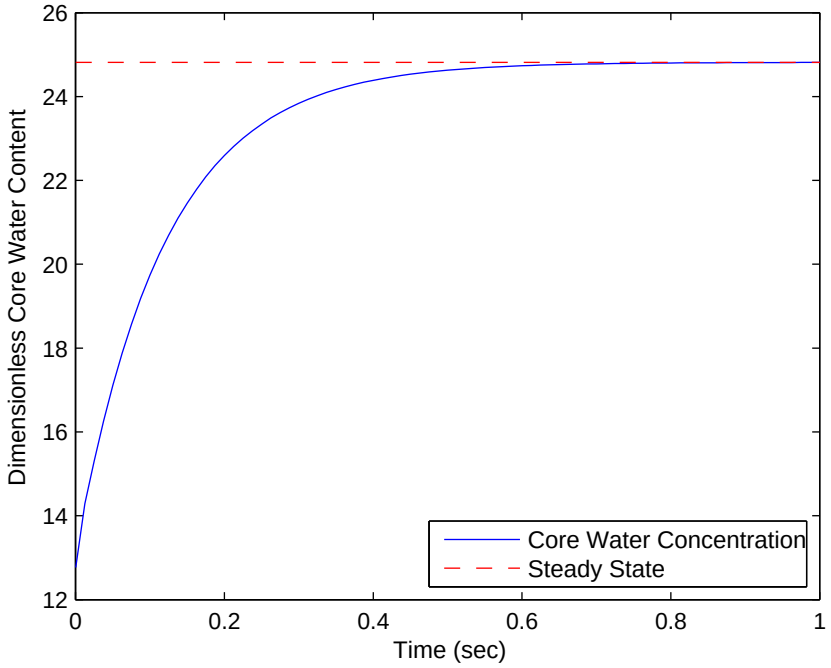

Figure 3.6: Core Water Concentration for γ=1 at 320 °C

Figure 3.6 maintains the same value for γ ($\gamma = 1$) but is analyzed at an initial release temperature of 320 °C. When compared to Figure 3.5, the long term core water level is essentially equivalent for both temperatures but the difference in initial water concentration is caused by the release of chemically bound water due to the higher temperature.

Now we will examine the evolution of the core water level when a spore is thermally treated via a wet heating process. Figure 3.7 shows the change in core water concentration at 320 °C for $\gamma = 10$. This implies that the water concentration outside the spore is much higher than inside the spore (wet heating). Note that the amount of water in the core increases rapidly to a much higher level as water is diffusing into the cortex and then into the core from outside the spore.

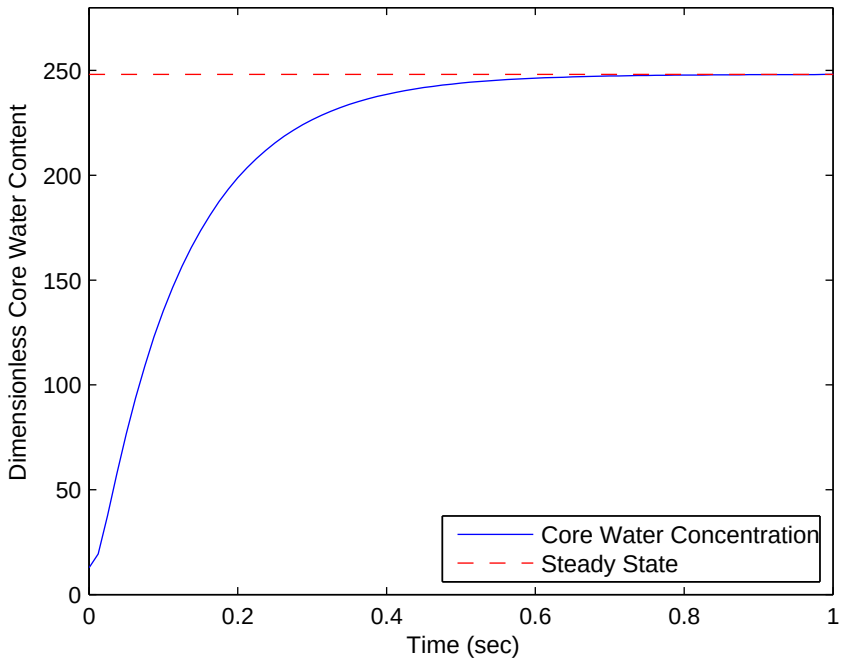

Figure 3.7: Core Water Concentration for γ=10 at 320 °C

Figure 3.8 demonstrates the evolution of the core water concentration for $\gamma = 0.1$, or a dry heating process, at 320 °C. This example clearly illustrates the limiting time behaviors. Initially the core water level rises since all the released absorbed

and chemically bound water in the cortex immediately flows outward. Keep in mind that the core does not contain any absorbed water so the cortex water concentration initially seeks to equilibrate by diffusing into the core. But as time progresses, the ratio of ambient humidity to spore water concentration becomes the dominating behavior and water flows out of the spore. In addition, the core water content level is much lower than the previous examples.

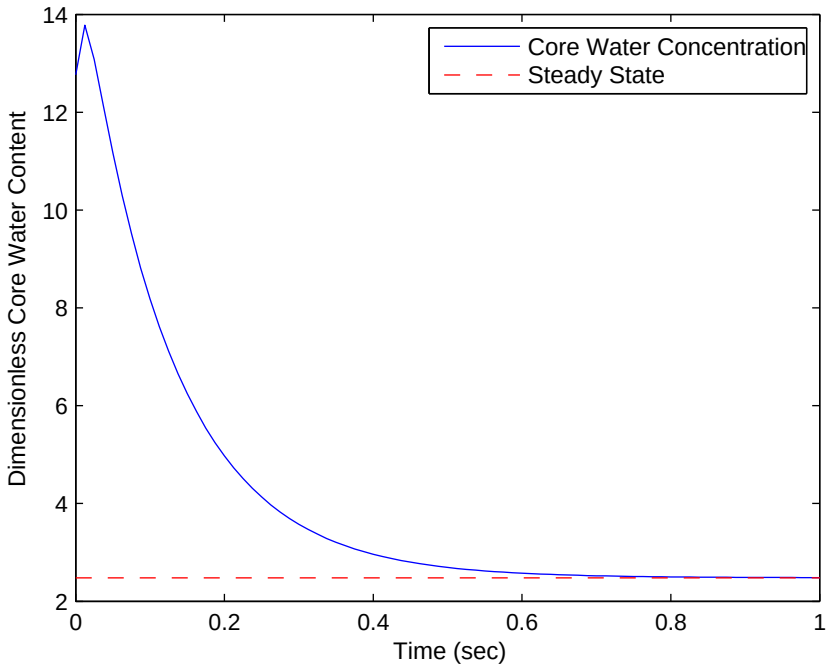

Figure 3.8: Core Water Concentration for γ=0.1 at 320 °C

As a comparison, Figure 3.9 graphs the core water concentration for the same value of γ but at an initial water release temperature of 110 °C. Since the lower temperature gives a constant value of released absorbed water within the spore, there is no initial water diffusion from the cortex into the core, just an equilibrium with the surrounding environment.

The release, diffusion, and reactions of water within a spore cause damage to a spore's DNA and proteins. The results of the water mobility model and subsequent

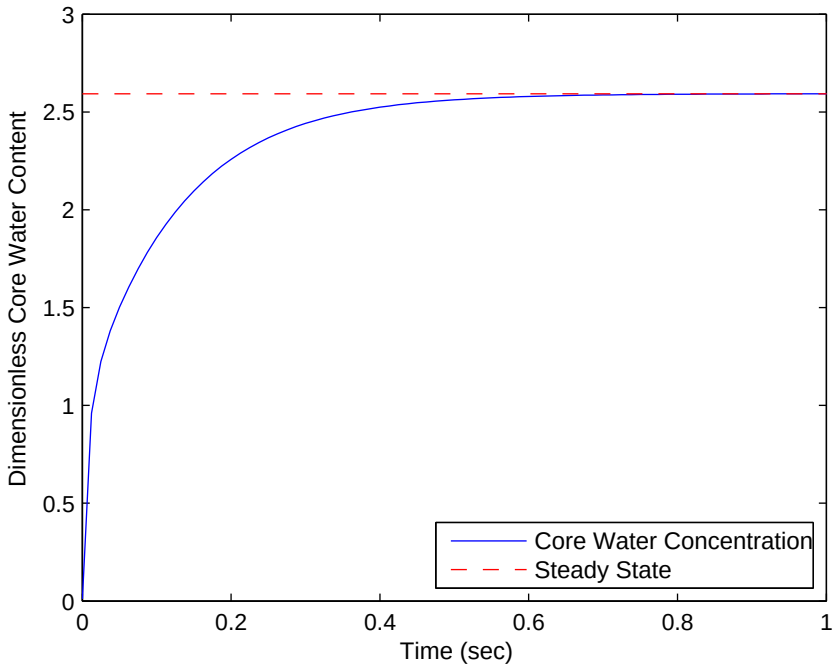

Figure 3.9: Core Water Concentration for γ=0.1 at 110 °C

damage due to hydrolysis reactions will now be utilized to characterize a spore's probability of kill.

IV. Probability of Kill Model

4.1 Introduction

Chapter III illustrated the release and mobility of water throughout a spore. This diffusion of water allows hydrolysis reactions to occur within the spore. As explained in the introduction, we contend that hydrolysis reactions leading to deploymerization of the spore's DNA and proteins will decimate these long chain molecules to such an extent that they can no longer be repaired. We further assume that damage to the spore is based on a certain initial protein fitness of the spore population. Once this fitness level is degraded beyond a critical level, the spore can no longer repair damaged DNA and thus cannot germinate, or produce outgrowth. These assertions allow us to create a probability of kill model based on water mobility, hydrolysis, DNA information content, and fitness levels of the spore's proteins.

4.2 Hydrolysis

Once water molecules become mobile and diffuse throughout a spore, chemical reactions occur. Hydrolysis is a reaction of a molecule with water. The acid or base environment for hydrolysis is important in the following way. Hydrolysis can be catalyzed by H^+ or by OH^-, so often rates of reaction can be represented as:

$$\text{Rate} = (k_H)\,[\text{Biomolecule}]$$

where k_H is the total reaction rate given by

$$k_H = k_A\left[H^+\right] + k_B\left[OH^-\right] + k_N$$

where

$$k_N = k_N^*\left[H_2O\right]$$

with

$$[\cdot] = \text{activity of ions}$$
$$k_A = \text{acidic rate}$$
$$k_B = \text{basic rate}$$
$$k_N = \text{neutral rate.}$$

The measurement of pH in a solution is related to its acidity or basicity. Bacteria can survive an environment with pH measurements between five and eight. A solution with a pH below seven is acidic and a pH above seven is basic. The rate of reaction of hydrogen molecules versus pH level is characterized by

$$\text{pH} = -\log\left[\text{H}^+\right]$$

and the rate of reaction with pH values close to seven is shown Figure 4.1 [12].

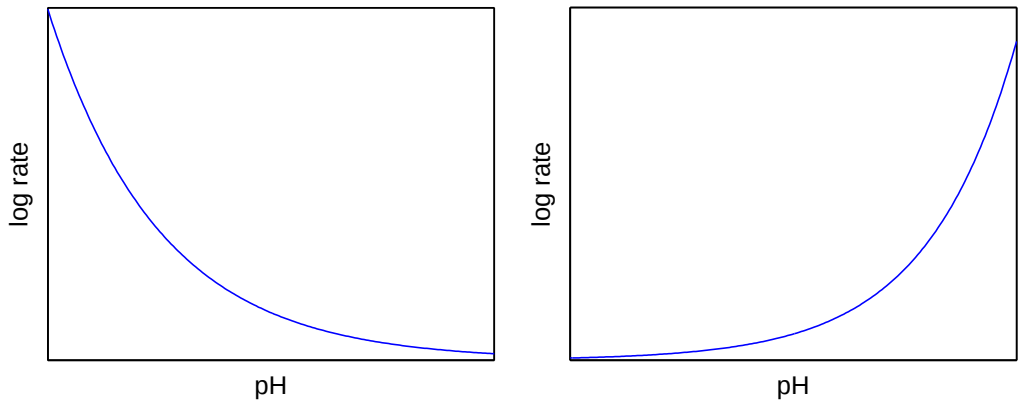

(a) Log rate versus pH of H^+. (b) Log rate versus pH of OH^-.

Figure 4.1: Log Rate of Reaction versus pH Level

The relationship between hydroxide molecules is related to the pH level by

$$-\log K_w = \text{pH} + \text{pOH}$$

where

$$K_w = \text{dissociation constant} \approx 10^{-14} \text{ at } 25\ ^\circ\text{C}.$$

Therefore a neutral solution that is neither acidic or basic has a concentration of hydrogen and hydroxide ions equal to 10^{-7}moles dm^{-3}. Note that the rates of reaction increase as the activity of negatively or positively charged ions increases [12]. More importantly, "microbial cells require their internal pH to remain constant in order to maintain essential cell functions" [41]. We assume that k_A and k_B are constant corresponding to a neutral acid/base environment and therefore k_N depends only on the rate of water activity.

As previously stated, water can react with biopolymers such as DNA and proteins resulting in depolymerization or removal of a side group of the polymer. Deploymerization is breaking a large strand of polymers into two smaller ones. Water can also react with DNA causing deamination and depurination damage. Deamination takes place when an amino group from the DNA's base pair is severed. This prevents the DNA from replicating properly. "Thus a change in the DNA base code would both propagate and replicate as the essential cell proteins would be improperly produced or not produced at all because of this DNA damage" [20].

DNA is most susceptible to depurination which occurs when DNA undergoes spontaneous decomposition in living cells. During depurination, a DNA base pair is removed from the DNA chain. When DNA is missing one of its base pairs, the DNA strand can not match up with its other half of the helix chain. Information is encoded in the DNA polymer as a series of base pairs. DNA contains the genetic information enabling organisms, including bacteria, to replicate. The information is encoded by the location of bases on the DNA backbone. Each of four bases along the DNA backbone represents a bit of information. Three bits encode for a letter in the DNA language, called a codon. A specific codon codes for a particular amino acid in its place along the length of a protein polymer during its synthesis. The information is preserved and replicated by the Watson-Crick base pairing in which

complementary bases recognize each other. One incorrect amino acid can dramatically alter the function of the protein, particularly shape sensitive proteins like enzyme catalysts. Three bits of ordered information allow 64 possible encoding combinations. The capability of the three-bit letter is more than sufficient to encode for 20 amino acids that make up proteins. Thus there exists redundancy in the code. As a result, removing or altering the third base pair in the sequence of three bits in a codon may or may not destroy the information content; removing the first base causes problems more frequently. Some codon letters are inactive, so destroying that information causes no degradation in function of the DNA or the proteins for which it codes. Hence, damage to a particular DNA base can have a range of effects depending on the information content of the codon or the information content of the bit within the codon. We limit ourselves to consider damage which reduces information content in critical or essential codons, which contain information necessary to replicate the spore during germination. Even so, there is a range of information degradation that can occur for each base that is damaged or removed [13]. We can account for this variability in our model by including a distribution of damage influences for each base that reacts by hydrolytic depurination or deamination.

Water reactions with proteins cause denaturation damage. Denaturation is a process in which proteins lose their structure by application of some external stress. Native structures of proteins may be altered, and their biological activity changed or destroyed by treatment that does not disrupt the primary structure. Following denaturation, some proteins will return to their native structures under proper conditions. Extreme conditions, such as strong heating, usually cause irreversible change. Since the structure of the protein determines its function, the protein can no longer perform its function once it has been denatured [37]. For the purpose of our research, we will assume that hydrolysis reactions are equally likely to occur at all protein sites. Further, we will assume that the critical threshold damage to DNA caused by depurination is equally likely for all base pair sites. The damage caused by hydrolysis reactions will be considered in the probability of kill model.

4.3 Probability of Kill Model

There exist many models describing the inactivation of *Bacillus* spores. These models, through use of various heating methods, relate time and temperature to the inactivation of spores. Refer to Figure 4.2 for a graphical representation of some of these models [17,44] where heating time is a log linear function. The data gathered by AFIT researchers, Goetz and Hawkins, used similar heating techniques as described in Chapter II [20,21]. Battelle used a series of furnaces to suspend spores in heat for various periods of time [2].

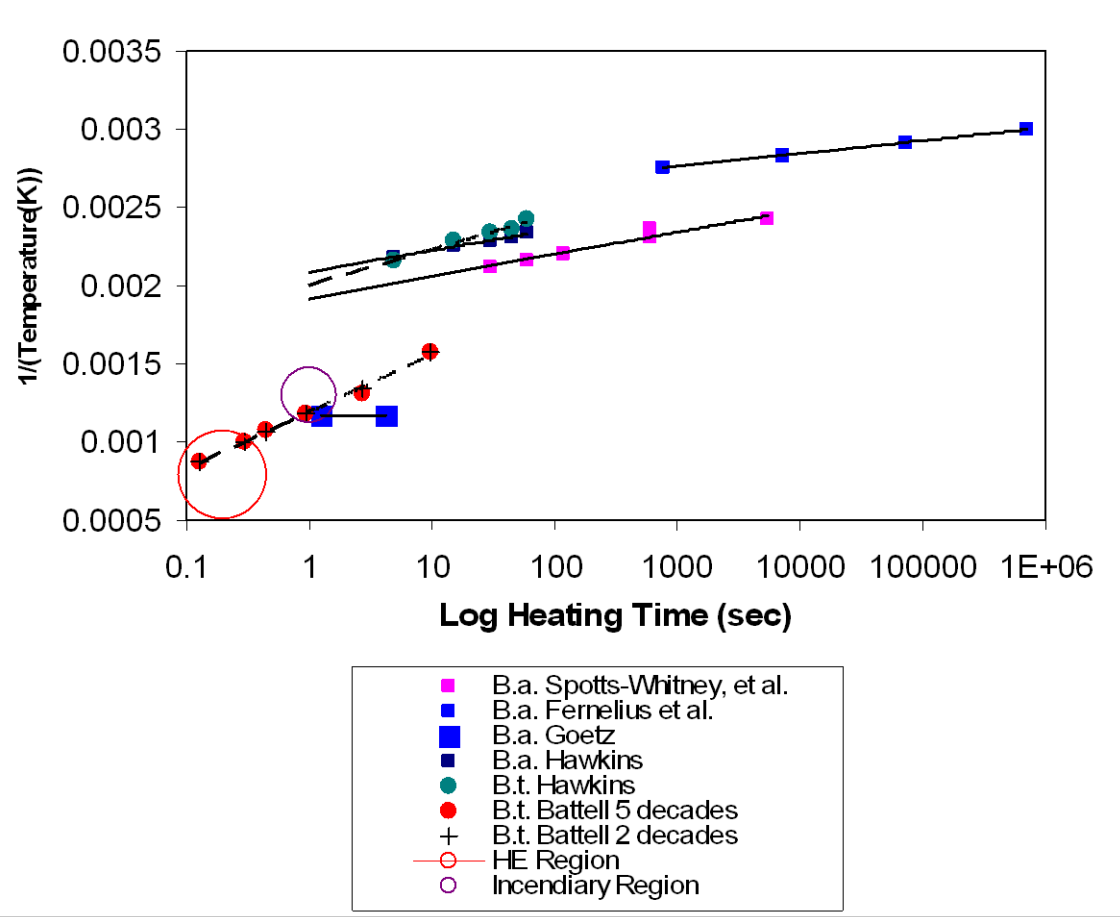

Figure 4.2: Heat Inactivation of *Bacillus* Spores

The Battelle data is the closest comparison found in the literature of short duration, high temperatures similar to the parameters utilized in this research. Notice that the slope of the heat inactivation of the Battelle data is different than the slope of inactivation when spores were heated at lower temperatures and for longer time periods.

Our model, while still taking into account the effects of heating temperature and duration, will also consider a third variable to explain the inactivation of spores. We suggest that diffusion of water throughout a spore, and thus the hydrolysis reactions with DNA and proteins, damage these molecules to such an extent that the spore is effectively dead. In addition, these hydrolysis reactions cause the difference in the heat inactivation slope when spores are heated at high temperatures and for short durations (refer to Figure 4.2) [7]. We assume that although hydrolysis reactions are equally likely to occur at all DNA sites, these hydrolysis reactions can occur multiple times causing the DNA to lose information content per hydrolysis event. Thus we propose that DNA information content is based on the effect of damage due to hydrolysis reactions. We further propose that a population of heat-treated spores has a certain initial 'fitness' distribution based on viability of protein and capacity to repair DNA, and by choosing one spore from the sample we are provided a specific protein fitness level. We offer a model which correlates spore inactivation with time, temperature, an initial DNA information content level within a particular spore, and an initial protein fitness distribution of the spore population.

Let $I_D(t)$ be the DNA information content in a given spore at time t. The rate of DNA damage caused by heating and hydrolysis will be modeled by

$$-\frac{\mathrm{d}I_D}{\mathrm{d}t} = k_1(T)I_D + k_2(T)\left[\mathrm{H_2O}\right]_c(t)I_D \tag{4.1}$$

where $[H_2O]_c(t)$ is defined by Equation (3.24) and

t =time

T =temperature

k_1 =rate coefficient associated with [DNA] breakdown during pyrolysis

k_2 =rate coefficient associated with [DNA] breakdown during hydrolysis.

This equation characterizes the rate of change in the DNA information content of a spore. The first term is the first order breakdown process associated with direct thermal pyrolysis reactions of DNA and the second term captures the influence of hydrolysis. The rate coefficients, $k_i(T)$, follow the Arrhenius equation [27]:

$$k_i(T) = A_i e^{-\frac{E_i}{RT}} \tag{4.2}$$

where A_i is the respective encounter frequency while E_i is the respective activation energy. By integrating with respect to time, Equation (4.1) becomes

$$I_D(t) = I_0 e^{-[k_1 t + k_2 H(t)]}$$

with

$$H(t) = \int_0^t [H_2O]_c(\tau) d\tau.$$

By using the core water concentration model in Equations (3.25) and (3.26) this becomes

$$H(t) = \frac{3}{x_c^3}[H_2O]_M \left\{ \sum_{n=1}^{\infty} F_n(T^*) G_n(x_c) \frac{1}{\omega_n} \left[1 - e^{-\omega_n t}\right] + \gamma \sum_{n=1}^{\infty} G_n(1) G_n(x_c) \frac{s_n^2}{\omega_n^2} \left[\omega_n t - \left(1 - e^{-\omega_n t}\right)\right] \right\}. \tag{4.3}$$

At time $t = 0$, the initial DNA information content, I_0, will be determined by a spore's DNA information content prior to heat treatment and subsequent hydrolysis. Since the DNA of one spore is nearly identical to that of another, the information content will be represented by a constant function. The information content will be degraded due to its hydrolytic susceptibility. "The death of the individual cell occurs when the number of functional ribosomes has dropped below a critical threshold level, beyond which the cell cannot recover" [41]. The same can be said for DNA. "While there can be repair of DNA damage...if too much damage has been accumulated during spore dormancy, this damage can overwhelm the capacity of repair systems and lead" to spore death [40]. Thus we let I_k denote the critical threshold such that if $I_D > I_k$, then the spore's DNA has enough viable information that it can be repaired and thus produce a cell during germination. See Figure 4.3 for an illustration of a spore's DNA information content prior to any heat treatment ($t = 0$).

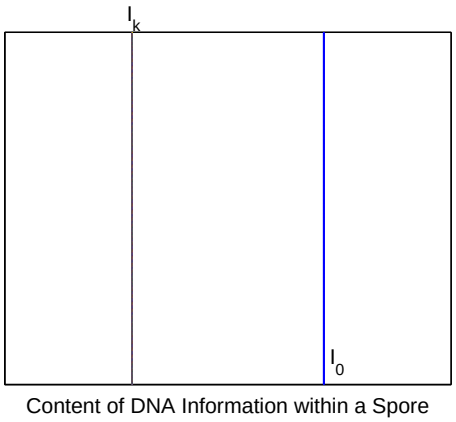

Figure 4.3: Spore DNA Information Content at $t = 0$

Let $I_D(\tau)$ be defined as the DNA information content at time $t = \tau$. As time progress, the probability that critical damage is done to a spore's DNA information content increases. We will assume this increase in critical damage follows a Gaussian density function with a mean of $\overline{I}_D$ and standard deviation designated as σ_D. The density function represents the hydrolytic susceptibility of DNA information con-

tent. Over time, σ_D increases as the likelihood of damage to an essential codon also increases. Figure 4.4 represents the degradation in DNA information content due to hydrolysis reactions as time evolves from $t = 0$ to $t = \tau_1$ then $t = \tau_2$, and I_D approaches its critical kill threshold, I_k.

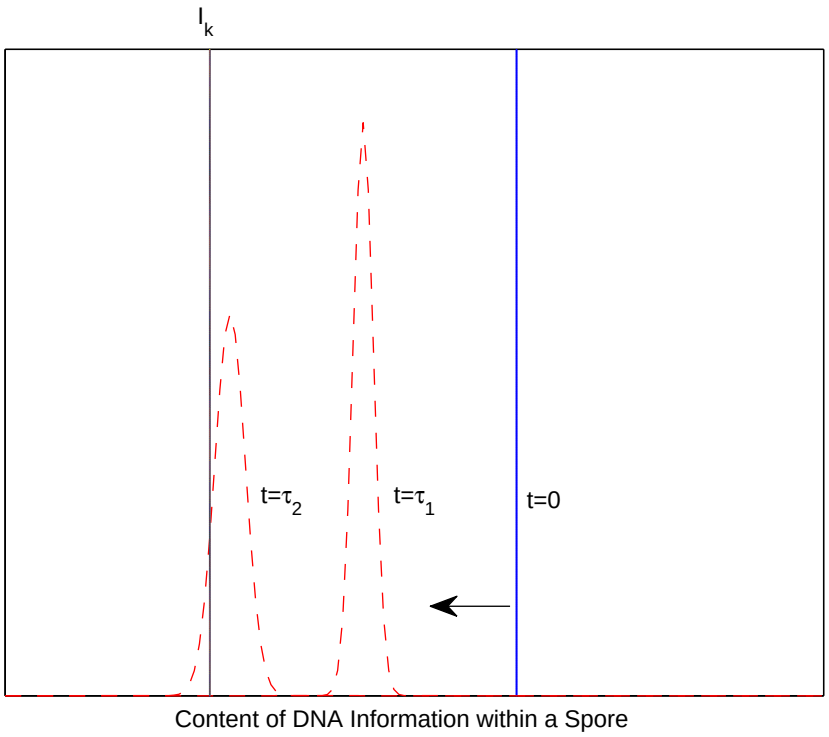

Figure 4.4: Spore DNA Information Content as it Evolves over Time

The probability density function for critical codon damage will not be considered in this research. Instead we assume any damage is critical codon damage. This leads to the conclusion that the spore is killed if $I_D \leq I_k$ and will survive if $I_D > I_k$. However, in addition to DNA damage, there is damage to proteins during heating and hydrolysis. Since proteins are necessary to repair DNA, a damaged spore will only be able to germinate with the protein that survives the heating process. So DNA must be repaired before a viable cell is produced during germination and there must be a suitable amount of repair protein available to accomplish this. Let $J_P(t)$ be the protein information content for the sample population at time t. The evolution

of protein content is also given by

$$-\frac{\mathrm{d}J_P}{\mathrm{d}t} = \tilde{k}_1(T)J_P + \tilde{k}_2(T)\left[\mathrm{H_2O}\right]_c(t)J_P \tag{4.4}$$

where

$\tilde{k}_1$ =rate coefficient associated with protein breakdown during pyrolysis

$\tilde{k}_2$ =rate coefficient associated with protein breakdown during hydrolysis

and the rate coefficients are also modeled by the Arrhenius equation (as in Equation 4.2).

At time $t = 0$, the initial protein information content, J_0, will be determined by the spore chosen from a population with a certain protein fitness distribution based on various preparation parameters. As previously discussed, spore preparation temperature effects the core water content which in turn influences a spore's heat resistance. In addition, "spores prepared at different temperatures have a number of significant differences in properties" besides heat resistance [19, 28]. Therefore due to the multitude of preparation parameters that affect the properties of a spore, our model will consider that a spore population will have a specified protein fitness distribution. We will model a spore's initial protein content via a Gaussian density function. At time $t = 0$, J_0, is randomly drawn from this function which has a mean of $\overline{J}_0$ and a standard deviation denoted by σ_P. See Figure 4.5 for an illustration of the protein fitness density function of a sample population of spores prior to any heat treatment ($t = 0$). After integration, Equation (4.4) becomes

$$J_P(t) = J_0 \mathrm{e}^{-\left[\tilde{k}_1 t + \tilde{k}_2 H(t)\right]}$$

with $H(t)$ given by Equation (4.3).

Proteins are needed to repair damaged DNA. For this reason, we are only concerned with repair proteins in the core because of the location of a spore's DNA.

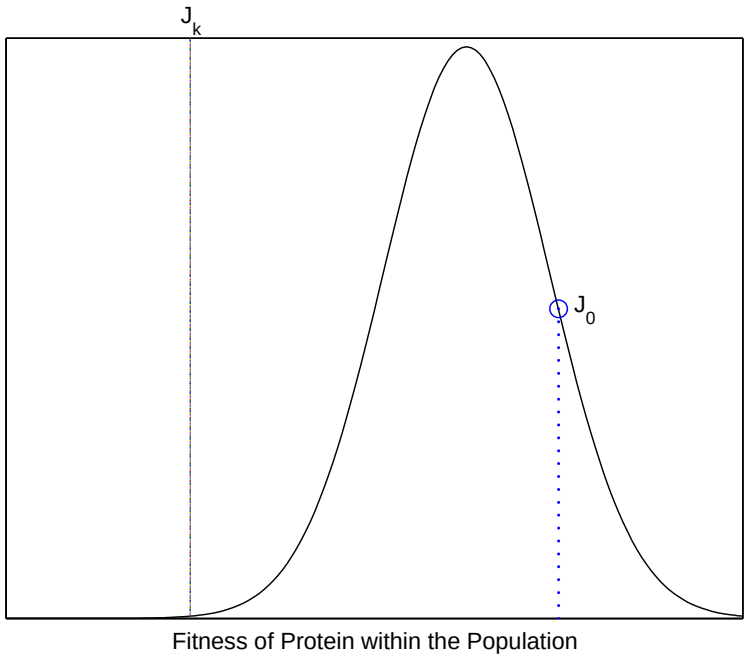

Figure 4.5: Sample Spore Population's Protein Fitness at $t = 0$

But proteins can also be degraded during heating and hydrolysis reactions and "this damage can overwhelm the capacity of repair systems and lead to" spore death [40]. Let J_k be the critical kill threshold such that when $J_P > J_k$, the spore contains the necessary repair protein information content in order to repair its DNA.

Since J_0 is a random variable drawn from the density function, $J_P(t)$ is also random. However, the standard deviation of $J_P(t)$, σ_P, is assumed to remain constant while the mean, $\overline{J}_P$, evolves with time since

$$\overline{J}_P(t) = \overline{J}_0 \mathrm{e}^{-[k_1 t + k_2 H(t)]}.$$

Let $J_P(\tau)$ be defined as the random variable taken from the density function which progresses to time $t = \tau$. Over time, J_P will approach its critical kill threshold, J_k. Refer to Figure 4.6 for a graphical representation.

In order to determine the probability of kill, P_k, for the spore, we simply need to integrate underneath the section of the Gaussian density function that has passed

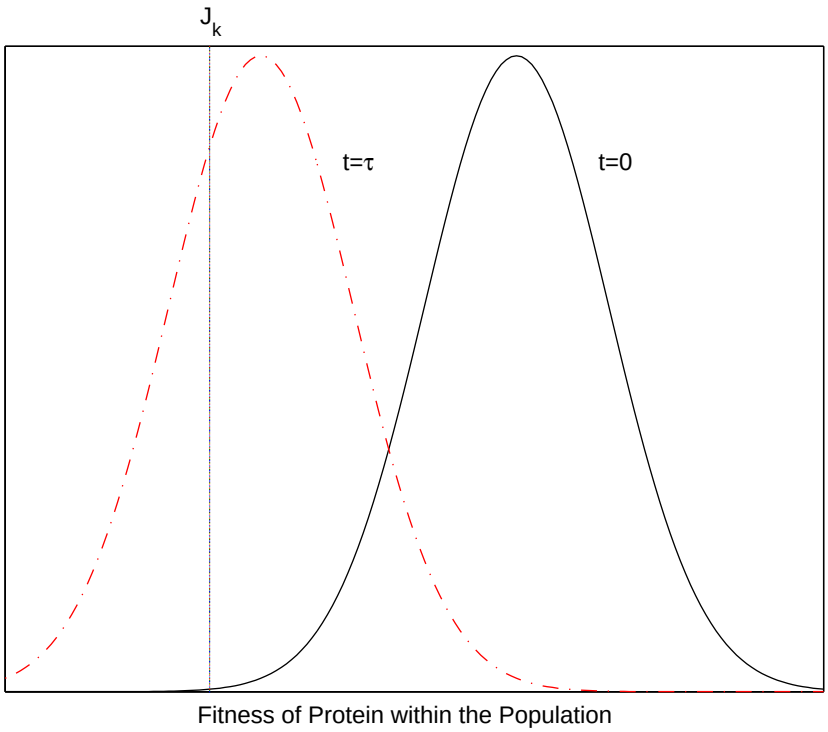

Figure 4.6: Sample Population's Protein Fitness as it Evolves over Time

the critical kill threshold:

$$P_k\left(J_\tau < J_k\right) = \frac{1}{\sqrt{2\pi}\sigma_P}\int_{-\infty}^{J_k} \mathrm{e}^{\left[-\frac{1}{2}\left(\frac{x-\overline{J}_\tau}{\sigma_P}\right)^2\right]}\mathrm{d}x. \tag{4.5}$$

Following integration Equation (4.5) becomes

$$P_k\left(J_\tau < J_k\right) = \tfrac{1}{2}\left[1 + \mathrm{erf}(Q_P)\right] \tag{4.6}$$

where

$$Q_P = \frac{J_k - \overline{J}_\tau}{\sqrt{2}\sigma_P}. \tag{4.7}$$

This probability of kill analysis will be evaluated to examine the influence of wet versus dry heating on a spore.

4.4 Results

The parameters used within the probability of kill model are found in Table 4.1 [15, 26, 29, 30, 48].

Table 4.1: Parameters for Probability of Kill Model

Parameter	Value	Units
R	1.986×10^{-3}	kcal/mol°K
A_1	2.0×10^{12}	sec^{-1}
E_1	65.683	kcal/mol
A_2	2.564×10^{10}	sec^{-1}
E_2	29	kcal/mol
$\widetilde{A}_1$	4.828×10^{15}	sec^{-1}
$\widetilde{E}_1$	38.3	kcal/mol
$\widetilde{A}_2$	1.6×10^{3}	sec^{-1}
$\widetilde{E}_2$	10	kcal/mol

Figure 4.7 illustrates the probability of protein survival with an initial release temperature, T^*, of 300 °C. The dashed line represents wet heating or $\gamma = 10$. The upper line reflects a dry heating process where $\gamma = 0.1$. Note that it takes twice as long (0.1 seconds versus 0.2 seconds) for the dry heating process to achieve a 90% reduction in protein population survival (see the values marked by a $*$). This supports the contention that an increased amount of hydrolysis reactions will cause faster protein damage. In fact, Figure 4.7 shows that at 0.1 seconds wet heating produced a 10% survival probability while the same exposure time with dry heating produced a 73% survival probability (shown by the $\circ$). Further, we see the survival probability curves see the asymptote to a constant value (approximately 0.25 seconds). Our results imply that the entire population can never be killed. This is a consequence of modeling the protein fitness with a Gaussian density function which approaches zero only at positive and negative infinity. Because $\overline{J}_\tau$ is bounded below by zero, Q_P in Equation (4.7) is bounded above by $J_k/\sqrt{2}\sigma_P$. This leads to a minimum survival

probability (using Equation (4.6)) of

$$1 - P_{k\,\min} = \tfrac{1}{2}\left[1 - \operatorname{erf}\left(\frac{J_k}{\sqrt{2}\sigma_P}\right)\right]$$

Logically we know that there exists a finite amount of information in the spore population's protein fitness and it should be possible to kill the entire population.

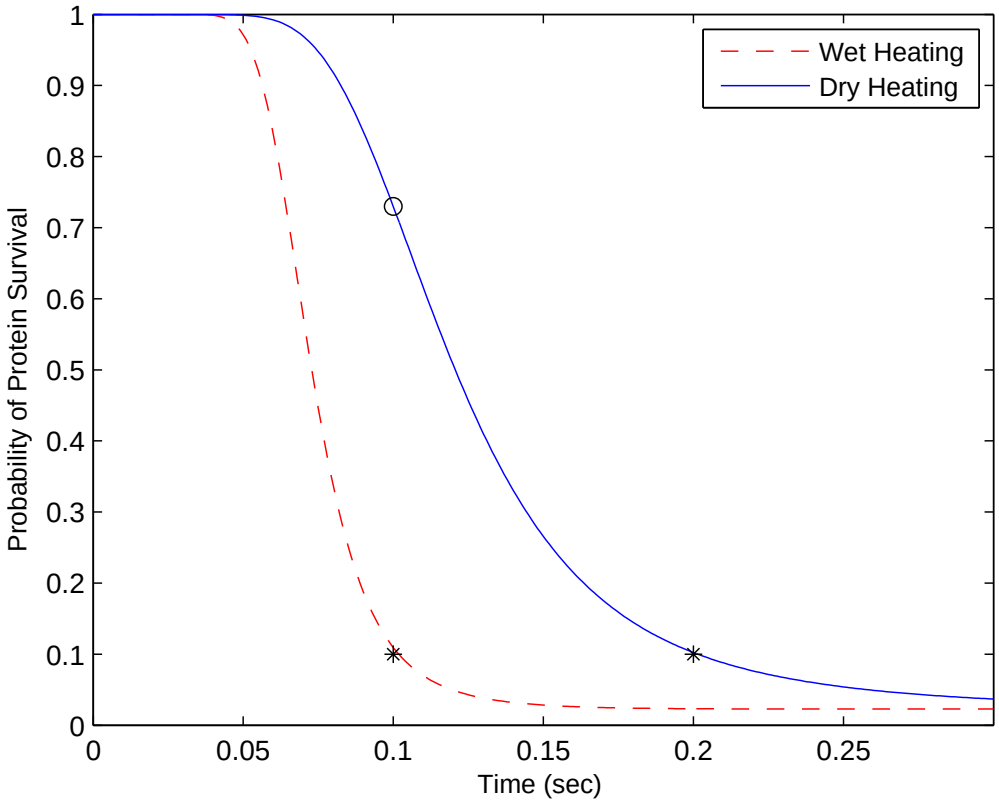

Figure 4.7: Probability of Protein Survival at 300 °C

The probability of protein survival during a wet heating process ($\gamma = 10$) at varying temperatures is shown in Figure 4.8. As expected, when heated at increasingly higher temperatures, equivalent protein damage takes place within a shorter duration. Notice that even at 200 °C the protein damage asymptote is reached by approximately 0.6 seconds. As shown in Section 3.5.2, this time duration will only reflect the influence of released water within the spore. The effect of ambient water concentration is not

reflected during these early time periods. Thus, the difference in the probability of kill measurements for various temperatures represents the concentration of absorbed and chemically bound water within the spore. For example, at 300 °C the release of chemically bound water causes the protein to be damaged faster as more water is available for hydrolysis reactions.

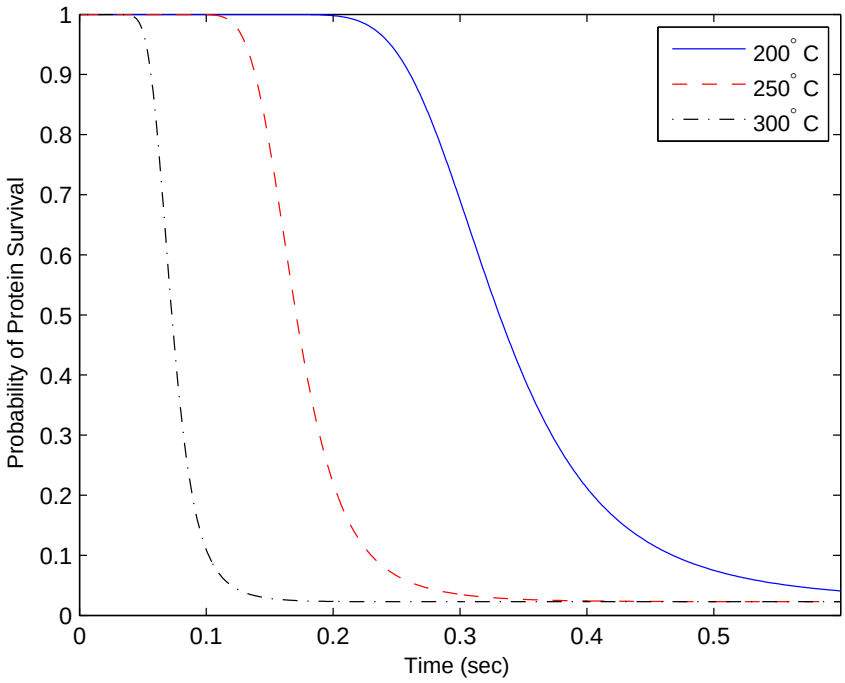

Figure 4.8: Probability of Protein Survival During Wet Heating

Figure 4.9 represents a dry heating process ($\gamma = 0.1$) for initial water release temperatures of 250 °C and 300 °C. The disparity between these two temperatures reflects the lesser amount of initial released water, as well as the influence of ambient humidity. Recall from Chapter III that after 0.6 seconds the outside water concentration dominates the diffusion of water throughout the spore. At $T^* = 250$ °C, some protein survives for up to five seconds as water is flowing from inside the spore into the surrounding environment and there is less water available for hydrolysis reactions within the core.

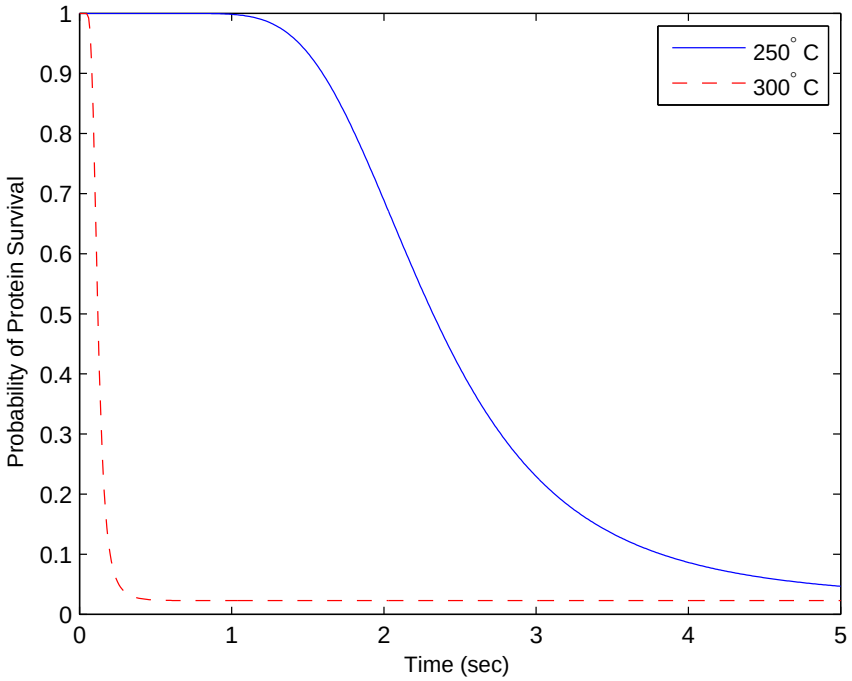

Figure 4.9: Probability of Protein Survival During Dry Heating

These results show the consequences of the release and diffusion of water throughout a *Bacillus* spore. Further, the production of water allows hydrolysis reactions to occur with the spore's DNA and proteins and these reactions may cause sufficient damage that the spore cannot be repaired. The probability of a spore being damaged to this extent can be represented by a probability of kill model.

V. Conclusions and Future Work

5.1 Conclusion

This research contains a notional characterization of damage to a *Bacillus* spore due to thermal heating and hydrolysis reactions. These hydrolysis reactions occur following the release and diffusion of water molecules throughout the spore which is effected by the type of heat treatment used (wet versus dry). Hydrolysis reactions damage a spore's DNA and proteins and the extent of this damage may result in the inability of the spore's DNA to be repaired and thus not germinate. Further, the damage of a spore can be represented as a probability of kill model.

Many assumptions were made during development of the probability of kill model. Throughout the entire research we assumed a spore was spherically symmetric. In addition, the rates of water release, water diffusion, and water consumption during hydrolysis reactions were similar to those found in recent studies but these rates were applied within this research which has not been replicated by laboratory experimentation. The actual distribution of absorbed and chemically bound water molecules within the spore also requires further exploration. These assumed parameters significantly impact the results of the probability of kill model and should be researched and analyzed in greater detail.

Under these assumptions the release, diffusion, and subsequent reactions of water within the spore's core were shown to be dependent on time, temperature, and water concentration of the outside environment. The temperature dictated the initial amount of water available for diffusion and hydrolysis reactions since absorbed water molecules were released as gaseous water molecules at approximately 100 °C while chemically bound water molecules are not released until 300 °C. At short time durations (less than 0.6 seconds) the distribution of absorbed and chemically bound water within the spore had the greatest influence on the core water concentration. After 0.6 seconds the surrounding environment's water concentration played a significant role in the transformation of the core water concentration.

Once the absorbed and chemically bound water molecules became available, their hydrolysis reactions with the spore's DNA and proteins caused deploymerization or removal of a side group of the polymer. This damage was modeled within a protein probability of kill model. A spore populations protein fitness was degraded due to hydrolysis reactions and an assumed critical kill threshold was utilized to determine if the protein was damaged to such an extent that it could not repair the spore's damaged DNA. The notional protein fitness density function and critical kill threshold impact the probability of kill model and also require further examination. The probability of protein survival depended whether a wet or dry heating process was utilized. A wet heating process allowed increased water flow into the spore and a greater amount of hydrolysis reactions thus protein damage takes place faster than during dry heating which causes water to flow from within the spore into the surrounding environment. Another parameter influencing the duration required to damage the entire population is the initial water release temperature. If this temperature is high enough to allow release of chemically bound water than protein is damaged more quickly since more water is available for hydrolysis reactions. This research provides a notional characterization of a spore's probability of kill depending on time, temperature, and hydrolysis reactions within the spore but further analysis is necessary to compare this research to real data.

5.2 Future Work

During development of the production/diffusion and probability of kill models contained in this research, the following areas were identified as requiring further analysis. Section 3.4.2 assumes a Gaussian density function for the release of absorbed and chemically bound water in a heat-treated spore. This is a valid assumption due to the Central Limit Theorem which states that any population with a significantly large sample size will have a sampling distribution that is approximately Gaussian. But a Gaussian density function approaches negative infinity as the probability of an event occurrence approaches zero. It does not take into consideration that if the

probability of an event occurring is zero, then the density function should reflect a value of zero. As spores are heated, water molecules might participate in hydrolysis reactions as soon as they are released which would indicated a release rate of zero, but the water release rate can never be negative. Therefore, further analysis and model development should examine the effects of various density functions for the release of water molecules. In particular, the Weibull density function has the added benefit that the density function is zero for when the probability of event occurrence is zero. Consequently, if no water is released then the probability of water being released is zero. Refer to Figure 5.1 for a graphical representation of a Weibull density function [45].

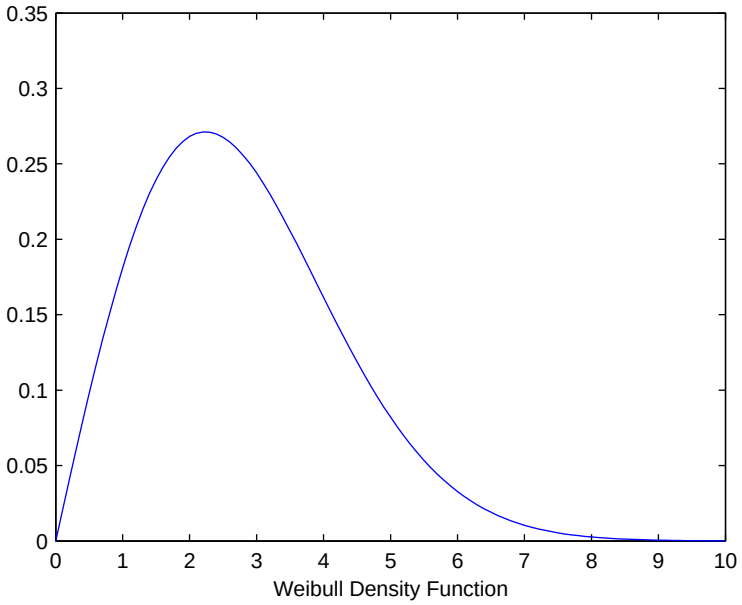

Figure 5.1: Weibull Density Function

Similarly, in Section 4.3, we assumed a Gaussian density function for protein fitness levels of a population of spores. We know logically there cannot exist a negative fitness level for this parameter. Protein fitness can be completely degraded to such an extent that the fitness level is zero, but it cannot be below zero. Thus a Weibull density function may also be an improved assumption for these parameter.

Further, the comparison of protein probability of kill to real data is difficult as reaction rate parameters are not well known. Another recommendation is to fit the known data with notional response behavior motivated by the model and examine the extrapolated model. Guided by the solution given in Equation (4.3), we could use the simplified model

$$H(t,T) = A(T)t + B(T)\left[1 - \mathrm{e}^{-\omega t}\right]$$

to represent the effect of hydrolysis. The coefficients A(T), B(T), and decay rate ω could be estimated from data. This rate function is then used in the kill probability model.

Within our probability of kill model, spore death is modeled by hydrolysis damage to DNA or proteins by means of a wet or dry heating process. Ishihara and others found that spores dehydrated to less than 22% of their initial bound water could not germinate [23]. Depending on the degree of degradation, DNA can be repaired by proteins. Therefore, future research should consider a spore outgrowth model based on the combined damage of DNA and proteins following heat treatment. If there exists sufficient protein that functions properly, can the DNA be repaired to a viable level such that spore replication and germination occur? And since this repair will involve protein synthesis, will the repair process decimate the protein fitness level to beyond its critical kill threshold such that spore death occurs? In other words, what quantities of viable DNA and proteins will allow the protein to repair DNA after experiencing heat damage? This approach could be mathematically modeled in a similar manner as the other processes contained in this research in order to develop a spore outgrowth model. In addition, an outgrowth model would allow improved comparisons with real data.

Rosenberg, Cavalieri, and Ungers propose the existence of repressor and anti-repressor proteins in a spore. They suggest that these proteins repress or initiate replication of DNA respectively leading to spore death or germination [35]. Rubinow

investigates an mathematical model of the accumulation rates of repressor proteins, anti-repressor proteins and the triggering of protein synthesis with DNA [36]. In order to extend the probability of kill model to include a spore outgrowth model, the proposed repressor and anti-repressor protein initiatives could be further analyzed.

Finally, this research only considers hydrolysis reactions with DNA and proteins. This concept could easily be extended to other reaction kinetics. The same analysis applies if treating a spore with chemicals other than water.

Appendix A. MATLAB Code for the Thermal Heating Model

The following appendix contains the MATLAB code used to numerically evaluate the thermal heating model in Chapter II:

```
function thesiscylindricalcoordv7test
clc;clear all;clf;

N=600;
dt=.00002; %Time step

%Radial direction; half of distance between adjacent spores
r=linspace(0,.8,(2*N/3));
dr=r(2)-r(1); %spatial step in r direction
rmesh=length(r); %develop uniform mesh

%Z direction; total width of glass slide and coverslip
z=linspace(-.2,1,N);
dz=z(2)-z(1); %spatial step in z direction
zmesh=length(z); %develop uniformmesh

%Set up ut=urr+(1/rj)*ur matrix, where rj=dr*j, Crank-Nicholson method
lambdar=dt/(dr.^2);
q=spdiags(repmat([1 -2 1],[rmesh 1]),-1:1,rmesh,rmesh)*lambdar;
UL3=dt./((2*dr.^2).*(1:rmesh));
UL4=dt./((2*dr.^2).*(0:rmesh-2));
UL4=[0,UL4];
q=(q-spdiags(UL3',-1,rmesh,rmesh));
q=(q+spdiags(UL4',1,rmesh,rmesh));
A=(speye(rmesh)+(0.5*q));
B=(speye(rmesh)-(0.5*q));
```

```
%ut=urr+(1/r)*ur boundary condition when r=0
B(1,1)=1+2*lambdar; B(1,2)=-2*lambdar;
A(1,1)=1-2*lambdar; A(1,2)=2*lambdar;

%Set up ut=uzz matrices, Crank-Nicholson method
%Due to Strang Splitting, z discretization is for half time step
dtz=dt/2;
lambdaz=dtz/(dz.^2);
Q=spdiags(repmat([1 -2 1],[zmesh 1]),-1:1,zmesh,zmesh)*lambdaz;
C=(speye(zmesh)+(0.5*Q));
D=(speye(zmesh)-(0.5*Q));

Bi=.0213; %Biot number where Bi=hl/K
lambdaBib=(Bi*dt)/(2-Bi*(dz^2)); %factor for bottom boundary conditions
lambdaBit=(-Bi*dt)/(2+Bi*(dz^2)); %factor for top boundary conditions

%Boundary Conditions for the uzz matrix:
%Lower BC, based on Newton's Law of Cooling
D(1,1)=1-lambdaBib; D(1,2)=0; C(1,1)=1-lambdaBib; C(1,2)=0;
%Upper boundary condition, based on Newton's Law of Cooling
D(zmesh,zmesh-1)=0; D(zmesh,zmesh)=1-lambdaBit;

u=zeros(zmesh,rmesh); %Initial Conditions (zero heat throughout domain)

%Solve ut=urr+(1/rj)*ur+uzz+S via Strang Splitting
for j=1:5256; %Run for 4000 loops to find solutions 1 & 3,
    %5256 loops to find solution 2 (see below)

%Set up source term, assign constant value for radius of source
    if j<2628 %Source 'on' for .12 sec
        source=sourcefun(zmesh,rmesh,dt);
```

```
    else
            source=zeros(zmesh,rmesh); %Turn source 'off' after .12 sec
    end

u=zdirection(C,D,u,source); %Solve in z direction for half time step
u=radial(A,B,u,source); %Solve in r direction for a full time step
u=zdirection(C,D,u,source); %Solve in z direction for half time step
end
end

function source=sourcefun(zmesh,rmesh,dt)
constant=zeros(zmesh,rmesh);
%Placement of source with 4 Micron depth & 36 Micron radius
constant(100,1:18)=dt*20; constant(101,1:18)=dt*20;
source=constant;
end

function firststep=zdirection(C,D,u,Source)
firststep=D\(C*u+0.25*Source);
end

function secondstep=radial(A,B,u,Source)
secondstep=(B\(A*u'+0.5*Source'))';
end
```

Appendix B. Details of Water Mobility Analytical Solution

The following appendix contains details of the analytical solution to the water production/diffusion model found in Chapter III. The original production/diffusion equation is

$$\frac{\partial w}{\partial t} = -k_t w + \nabla \cdot D\nabla w. \tag{B.1}$$

With one dimension, the diffusion term in Equation (B.1) becomes

$$\nabla \cdot D\nabla w = \frac{1}{r^2}\frac{\partial}{\partial r}\left(Dr^2\frac{\partial w}{\partial r}\right) \tag{B.2}$$

and because D is constant, Equation (B.2) is actually

$$\nabla \cdot D\nabla w = D\left(\frac{\partial^2 w}{\partial r^2} + \frac{2}{r}\frac{\partial w}{\partial r}\right). \tag{B.3}$$

At this point, we introduce dimensionless variables by choosing characteristic scales for length, time, and water concentration. We scale all by the spore radius, r_o; time by the diffusion time, $t_c = r_o^2/D$; and water concentration by the maximum concentration of the initial released water, $[H_2O]_M$, for any given temperature, T^*, i.e. $[H_2O]_M = \max_{0<r<r_o}[H_2O]_g(r, T^*)$. We define dimensionless variables x, τ, and v by

$$r = r_o x, \qquad t = t_c \tau, \qquad \text{and} \qquad w(r,t) = [H_2O]_M\, v(x,\tau). \tag{B.4}$$

Therefore, with the dimensionless variables, Equation (B.3) becomes

$$\begin{aligned}\nabla \cdot D\nabla w &= D[H_2O]_M\left(\frac{\partial^2 v}{\partial x^2}\frac{1}{r_o^2} + \frac{2}{x r_o^2}\frac{\partial v}{\partial x}\right)\\ &= \frac{D}{r_o^2}[H_2O]_M\left(\frac{\partial^2 v}{\partial x^2} + \frac{2}{x}\frac{\partial v}{\partial x}\right)\\ &= \frac{D}{r_o^2}[H_2O]_M\frac{1}{x^2}\frac{\partial}{\partial x}\left(x^2\frac{\partial v}{\partial x}\right).\end{aligned} \tag{B.5}$$

Inserting Equation (B.5) and other dimensionless variables into Equation (B.1) gives

$$\frac{[H_2O]_M}{t_c}\frac{\partial v}{\partial \tau} = -k_t [H_2O]_M v + \frac{D}{r_o^2}[H_2O]_M \frac{1}{x^2}\frac{\partial}{\partial x}\left(x^2\frac{\partial v}{\partial x}\right)$$
$$\frac{\partial v}{\partial \tau} = -\beta v + \frac{1}{x^2}\frac{\partial}{\partial x}\left(x^2\frac{\partial v}{\partial x}\right)$$

where

$$\beta = \frac{r_o^2 k_t}{D}.$$

With dimensionless variables, the original outer boundary condition,

$$-D\frac{\partial w}{\partial r}(r_o, t) = h\{w(r_o, t) - [H_2O]_a\} \tag{B.6}$$

becomes

$$-\frac{D}{r_o}[H_2O]_M \frac{\partial v}{\partial x}(1,\tau) = h\{[H_2O]_M v(1,\tau) - [H_2O]_a\}$$
$$-\frac{\partial v}{\partial x}(1,\tau) = B(v(1,\tau) - \gamma)$$

in which the total radius of the spore is scaled to the dimensionless value of 1,

$$B = \frac{r_o h}{D}, \qquad \text{and} \qquad \gamma = \frac{[H_2O]_a}{[H_2O]_M}.$$

In addition, the initial condition ($t = 0$),

$$w(r,0) = [H_2O]_g(r) = [H_2O]_\ell(r) f_1(T^*) + [H_2O]_b(r) f_2(T^*)$$

with dimensionless variables becomes

$$v(x,0) = \frac{w(r_o x, 0)}{[H_2O]_M} = \frac{[H_2O]_\ell}{[H_2O]_M}(r_o x) f_1(T^*) + \frac{[H_2O]_b}{[H_2O]_M}(r_o x) f_2(T^*)$$
$$= \alpha_1(x) f_1(T^*) + \alpha_2(x) f_2(T^*)$$

where

$$\alpha_1(x) = \frac{[\mathrm{H_2O}]_\ell}{[\mathrm{H_2O}]_M}(r_o x) \qquad \text{and} \qquad \alpha_2(x) = \frac{[\mathrm{H_2O}]_b}{[\mathrm{H_2O}]_M}(r_o x).$$

In summary, the dimensionless production/diffusion equation with boundary conditions and initial conditions is

$$\frac{\partial v}{\partial \tau} = -\beta v + \frac{1}{x^2}\frac{\partial}{\partial x}\left(x^2 \frac{\partial v}{\partial x}\right) \qquad 0 < x < 1,\ \tau > 0 \tag{B.7}$$

$$\frac{\partial v}{\partial x}(0,\tau) = 0 \qquad \tau > 0 \tag{B.8}$$

$$-\frac{\partial v}{\partial x}(1,\tau) = B(v(1,\tau) - \gamma) \qquad \tau > 0 \tag{B.9}$$

$$v\,(x,0) = \alpha_1\,(x)\,f_1\,(T^*) + \alpha_2(x) f_2\,(T^*) \qquad 0 < x < 1. \tag{B.10}$$

To solve this system of equations, we will use separation of variables. Let

$$v\,(x,\tau) = g\,(x)\,h\,(\tau)\,,$$

then Equation (B.7) becomes

$$g(x)h'(\tau) = -\beta h(\tau)g(x) + h(\tau)\frac{1}{x^2}\frac{\partial}{\partial x}\left[x^2 g'(x)\right]. \tag{B.11}$$

Let

$$\frac{h'(\tau) + \beta h(\tau)}{h(\tau)} = \frac{\frac{1}{x^2}\left([x^2 g'(x)]'\right.}{g(x)} \equiv -\mu,$$

where μ ia a separation parameter. Thus Equations (B.7), (B.8), and (B.9) become

$$h'(\tau) + (\beta + \mu)h(\tau) = 0 \tag{B.12}$$

$$\frac{1}{x^2}\left[x^2 g'(x)\right]' + \mu g(x) = 0 \tag{B.13}$$

$$g'(0) = 0 \tag{B.14}$$

$$-g'(1) = B\,g(1). \tag{B.15}$$

To simplify the solution to Equations (B.13), (B.14), and (B.15), let

$$g(x) = \frac{J(x)}{x}$$

then

$$g'(x) = \frac{xJ'(x) - J(x)}{x^2} \tag{B.16}$$

or

$$x^2 g'(x) = xJ'(x) - J(x).$$

Since

$$x^2 g(x) = xJ(x),$$

Equation (B.13) is reduced as

$$\begin{aligned} [xJ'(x) - J(x)]' + \mu x J(x) &= 0 \\ J'(x) + xJ''(x) - J'(x) + \mu x J(x) &= 0 \\ J''(x) + \mu J(x) &= 0. \end{aligned}$$

The solution to this differential equation is of the form

$$J(x) = A_1 \cos(sx) + A_2 \sin(sx)$$

where $s = \sqrt{\mu}$. Substituting into Equation (B.16),

$$\begin{aligned} g'(x) &= \frac{-A_1 sx \sin(sx) + A_2 sx \cos(sx) - A_1 \cos(sx) - A_2 \sin(sx)}{x^2} \\ &= -A_1 s^2 \left[\frac{sx \sin(sx) + \cos(sx)}{(sx)^2}\right] + A_2 s^2 \left[\frac{sx \cos(sx) - \sin(sx)}{(sx)^2}\right]. \end{aligned}$$

To satisfy Equation (B.14), $\lim_{x\to 0^+} g'(x) = 0$ requires $A_1 = 0$. Further, Equation (B.15) becomes

$$\begin{aligned} g'(1) + B\, g(1) &= J'(1) - J(1) + B\, J(1) \\ &= A_2 \left[s\cos(s) - (1-B)\sin(s) \right] \\ &= 0 \end{aligned}$$

For $A_2 \neq 0$ we require

$$s\cos(s) - (1-B)\sin(s) = 0$$

or

$$\tan(s) = \frac{s}{1-B} \tag{B.17}$$

provided $B \neq 1$. If $B = 1$ then we require $\cos(s) = 0$ or $s_n = (2n-1)\frac{\pi}{2}$. This same result is found in the limit as $B \to 1$ in Equation (B.17). Therefore, the eigenvalues and eigenfunctions associated with Equations (B.13), (B.14), and (B.15), with respect to the homogeneous boundary conditions, are of the form

$$g_n(x) = K_n \frac{\sin(s_n x)}{x} \qquad\qquad n \in \mathbb{N} \tag{B.18}$$

where the constant K_n is found by normalizing g_n and the eigenvalues, s_n, are determined by satisfying Equation (B.17). Figure B.1 represents a graphical solution to this equation for values of B equal to 0.2 and 5. It shows the intersection of the line $y = s/(1-B)$ with the tangent function. The points of intersection determine the eigenvalues. Note that the eigenvalues for $B = 0.2$ are indicated by a $+$ sign on the x-axis while a $\circ$ sign represents the eigenvalues for $B = 5$. Further, we see as n increases, the value of s_n approaches $(2n-1)\pi/2$. In fact a good approximation for large values of n is

$$s_n \approx (2n-1)\frac{\pi}{2} - \tan^{-1}\left[\frac{1-B}{(2n-1)\frac{\pi}{2}} \right].$$

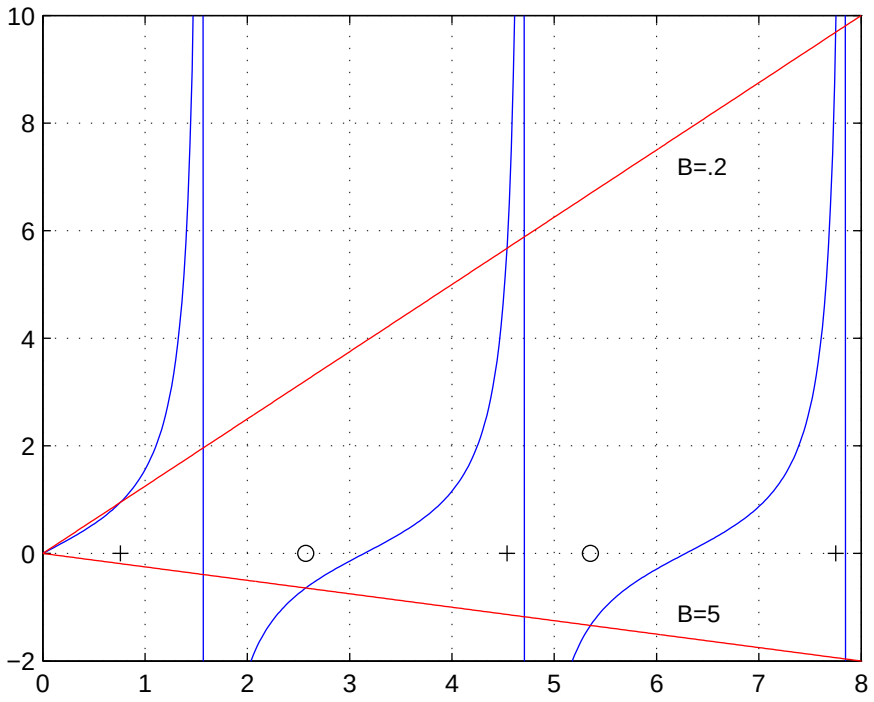

Figure B.1: Eigenvalues For B Equal to 0.2 and 5

Table B.1 presents the first eight values of s_n for various values of B between 0.2 and 10. Note as n increases, the eigenvalue approaches $(2n-1)\pi/2$ and the sequence converges to this value faster for large values of B. Figure B.2 graphically illustrates the values of s with n equal to 1, 2, and 3 as B varies from 0 to 10. These eigenfunctions are orthonormal with respect to the weight x^2, i.e.

$$\langle g_n, g_m \rangle = \int_0^1 x^2 g_n(x) g_m(x) \mathrm{d}x = \delta_{mn}.$$

To prove that g_n and g_m are orthogonal we use the ordinary differential equation (Equation (B.21)) for both g_n and g_m in self-adjoint form. We observe

$$\begin{aligned} \left(s_m^2 - s_n^2\right) x^2 g_n g_m &= g_n \left(x^2 g_m'\right)' - g_m \left(x^2 g_n'\right)' \\ &= \left[x^2 \left(g_n g_m' - g_m g_n'\right)\right]'. \end{aligned}$$

Table B.1: S_n for Various Values of B

$n \backslash B$	0.2	1	5	10
1	0.7593	1.5708	2.5704	2.8363
2	4.5379	4.7124	5.3540	5.7172
3	7.7511	7.8540	8.3029	8.6587
4	10.9225	10.9956	11.3348	11.6532
5	14.0804	14.1372	14.4080	14.6869
6	17.2324	17.2788	17.5034	17.7481
7	20.3811	20.4204	20.6120	20.8282
8	23.5280	23.5619	23.7289	23.9218

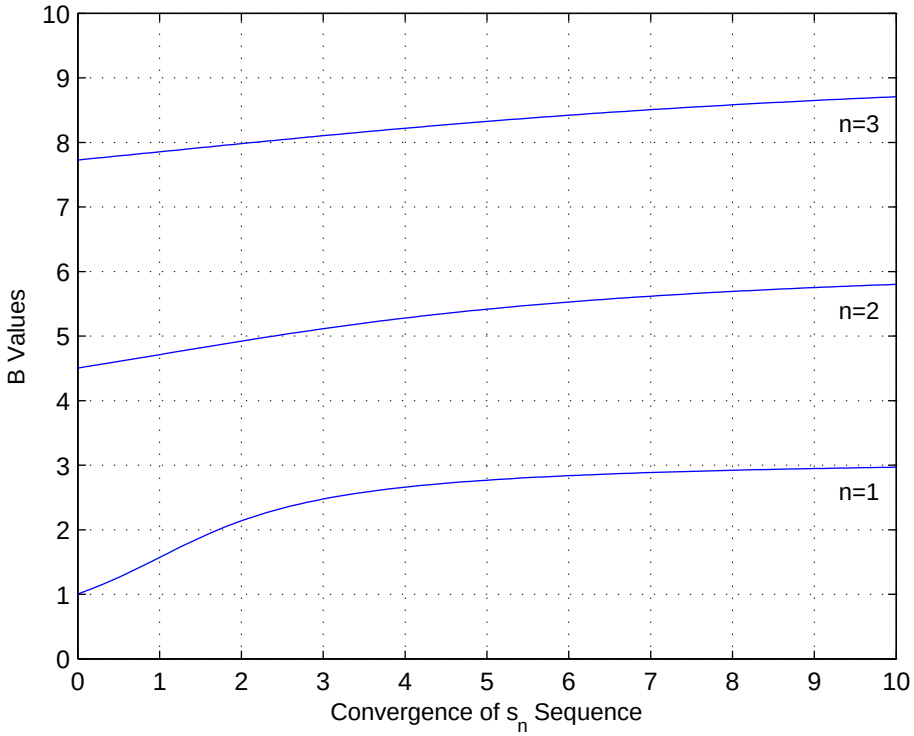

Figure B.2: S for $n = 1, 2, 3$ as B Increases From 1 to 10

Integrating leaves

$$\begin{aligned}\left(s_m^2 - s_n^2\right)\int_0^1 x^2 g_n g_m \mathrm{d}x &= x^2\left(g_n g_m' - g_m g_n'\right)\Big|_0^1 \\ &= g_n(1)g_m'(1) - g_m(1)g_n'(1) \\ &= 0\end{aligned}$$

which follows from Equations (B.22) and (B.23). So for $m \neq n$, $\langle g_n, g_m \rangle = 0$. To normalize g_n we choose K_n such that

$$\begin{aligned} 1 &= \int_0^1 x^2 g_n^2 \mathrm{d}x \\ &= \int_0^1 K_n^2 \sin^2(s_n x) \mathrm{d}x \end{aligned}$$

and by trigonometric identities,

$$1 = \frac{K_n^2}{2} \int_0^1 1 - \cos(2 s_n x) \mathrm{d}x.$$

Integrating implies

$$\begin{aligned} 1 &= \frac{K_n^2}{2} \left[1 - \frac{1}{2 s_n} \sin(2 s_n) \right] \\ &= \frac{K_n^2}{2} \left[1 - \frac{1}{s_n} \cos(s_n) \sin(s_n) \right]. \end{aligned} \tag{B.19}$$

Equation (B.17) allows

$$\sin(s_n) = \frac{s_n}{1 - B} \cos(s_n)$$

which lets Equation (B.19) become

$$\begin{aligned} &= \frac{K_n^2}{2} \left[1 - \frac{\cos^2(s_n)}{1 - B} \right] \\ &= \frac{K_n^2}{2(1 - B)} \left[\sin^2(s_n) - B \right]. \end{aligned}$$

Therefore, let

$$K_n = \sqrt{\frac{2(1 - B)}{\sin^2(s_n) - B}}.$$

and for this value of K_n, $\langle g_n, g_m \rangle = \delta_{mn}$. Notice that by applying Equation (B.17), $\lim_{B \to 1} K_n = \sqrt{2}$.

We next look for a solution in the form of the expansion

$$v(x,\tau) = \gamma + \sum_{n=1}^{\infty} h_n(\tau) g_n(x) \tag{B.20}$$

where $g_n(x)$ satisfies

$$\frac{1}{x^2}\left[x^2 g_n^{'}(x)\right]^{'} + s_n^2 g_n(x) = 0 \tag{B.21}$$

$$g_n^{'}(0) = 0 \tag{B.22}$$

$$g_n^{'}(1) + B\, g_n(1) = 0. \tag{B.23}$$

Further, with this choice of v, the boundary conditions are satisfied. Introducing Equation (B.20) back into Equation (B.7) gives

$$\sum_{n=1}^{\infty} h_n^{'}(\tau) g_n(x) = -\beta\gamma - \sum_{n=1}^{\infty} \beta h_n(\tau) g_n(x) + \sum_{n=1}^{\infty} h_n(\tau) \frac{1}{x^2}\left[x^2 g_n^{'}(x)\right]^{'}$$

which leads to

$$\sum_{n=1}^{\infty} \left[h_n'(\tau) + \beta h_n(\tau) + s_n^2 h_n(\tau)\right] g_n(x) = -\beta\gamma$$

and by orthogonality of $\{g_n\}$

$$h_n'(\tau) + \omega_n h_n(\tau) = -\beta\gamma \left\langle 1, g_n \right\rangle \tag{B.24}$$

where

$$\omega_n = \beta + s_n^2. \tag{B.25}$$

Finally, the initial conditions are determined from

$$\gamma + \sum_{n=1}^{\infty} h_n(0) g_n(x) = \alpha_1(x) f_1(T^*) + \alpha_2(x) f_2(T^*)$$

and the orthogonality of g_n allows us to obtain

$$h_n(0) = F_n(T^*) - \gamma \langle 1, g_n \rangle \tag{B.26}$$

where

$$F_n(T^*) = f_1(T^*) \langle \alpha_1, g_n \rangle + f_2(T^*) \langle \alpha_2, g_n \rangle .$$

Equation (B.24) along with the initial conditions produces the solution to the first-order differential equation:

$$\begin{aligned} h_n(\tau) &= \left[F_n(T^*) - \gamma \langle 1, g_n \rangle\right] \mathrm{e}^{-\omega_n \tau} + \int_0^\tau \mathrm{e}^{-\omega_n (t-\xi)} \left[-\beta\gamma \langle 1, g_n \rangle\right] \mathrm{d}\xi \\ &= F_n(T^*)\mathrm{e}^{-\omega_n \tau} - \gamma \langle 1, g_n \rangle \mathrm{e}^{-\omega_n \tau} - \frac{\beta\gamma \langle 1, g_n \rangle}{\omega_n} \left[1 - \mathrm{e}^{-\omega_n \tau}\right] . \end{aligned} \tag{B.27}$$

By utilizing Equation (B.25), Equation (B.27) is reduced to

$$h_n(\tau) = F_n(T^*)\mathrm{e}^{-\omega_n \tau} - \frac{\gamma \langle 1, g_n \rangle}{\omega_n} \left[\beta + s_n^2 \mathrm{e}^{-\omega_n \tau}\right] . \tag{B.28}$$

Next we observe that

$$\gamma = \sum_{n=1}^{\infty} \gamma \langle 1, g_n \rangle g_n(x),$$

which indicates that Equation (B.20) can be converted to

$$v(x, \tau) = \sum_{n=1}^{\infty} \left[h_n(\tau) + \gamma \langle 1, g_n \rangle\right] g_n(x). \tag{B.29}$$

Equation (B.28) implies

$$\begin{aligned} h_n(\tau) + \gamma \langle 1, g_n \rangle &= F_n(T^*)\mathrm{e}^{-\omega_n \tau} + \gamma \langle 1, g_n \rangle \left[1 - \frac{\beta}{\omega_n} - \frac{s_n^2}{\omega_n}\mathrm{e}^{-\omega_n \tau}\right] \\ &= F_n(T^*)\mathrm{e}^{-\omega_n \tau} + \gamma \langle 1, g_n \rangle \frac{s_n^2}{\omega_n} \left[1 - \mathrm{e}^{-\omega_n \tau}\right] \end{aligned} \tag{B.30}$$

where we again make use of Equation (B.25). Equations (B.29) and (B.30) allow us to state

$$v(x,\tau) = \sum_{n=1}^{\infty} F_n(T^*)\mathrm{e}^{-\omega_n \tau} g_n(x) + \gamma \sum_{n=1}^{\infty} \langle 1, g_n \rangle \frac{s_n^2}{\omega_n} \left[1 - \mathrm{e}^{-\omega_n \tau}\right] g_n(x). \tag{B.31}$$

To determine the average core water concentration we find the total core water and divide by the core volume ($V_{\text{core}} = \frac{4}{3}\pi r_c^3$)

$$\begin{aligned}
\left[\mathrm{H_2O}\right]_c(t) &= \frac{1}{V_{\text{core}}} \int_0^{r_c} \int_0^{2\pi} \int_0^{\pi} w(r,t) r^2 \sin(\phi) \mathrm{d}\phi \mathrm{d}\theta \mathrm{d}r \\
&= \frac{3}{r_c^3} \int_0^{r_c} w(r,t) r^2 \mathrm{d}r.
\end{aligned} \tag{B.32}$$

Now define $x_c = r_c/r_o$ and use the dimensionless variables in Equation (B.4) such that Equation (B.32) becomes

$$\left[\mathrm{H_2O}\right]_c(t_c\tau) = \frac{3}{x_c^3} \left[\mathrm{H_2O}\right]_M \int_0^{x_c} v(x,\tau) x^2 \mathrm{d}x.$$

Through use of Equation (B.31) we obtain

$$\begin{aligned}
\left[\mathrm{H_2O}\right]_c(t_c\tau) = \frac{3}{x_c^3} \left[\mathrm{H_2O}\right]_M \Bigg\{ &\sum_{n=1}^{\infty} F_n(T^*) G_n(x_c) \mathrm{e}^{-\omega_n \tau} \\
&+ \gamma \sum_{n=1}^{\infty} G_n(1) G_n(x_c) \frac{s_n^2}{\omega_n} \left[1 - \mathrm{e}^{-\omega_n \tau}\right] \Bigg\}
\end{aligned}$$

where

$$G_n(x) = \int_0^x \xi^2 g_n(\xi) \mathrm{d}\xi$$

and we observe $G_n(1) = \langle 1, g_n \rangle$.

Bibliography

1. Abramowitz, M., and Stegun, I.A. *Handbook of Mathematical Functions with Formulas, Graphs, and Mathematical Tables (10th Edition).* New York: Dover Publications, Inc., 1972.

2. Alexander, C. A., Ogden, J.S., LeVere, M.A., Dye, C.F., and Kohler, D.F. "Thermal Deactivation of Aerosolized Bacteria," Defense Threat Reduction Agency. Alexandria VA, (January 2007).

3. United States Department of Justice. "Amerithrax Investigation" Federal Bureau of Investigation, 2008. 12 January 2009 http://www.fbi.gov/anthrax/amerithraxlinks.htm.

4. Consensus Statement. "Anthrax as a Biological Weapon, 2002: Updated Recommendations for Management," *The Journal of the American Medical Association,* Vol. 287: No. 17, 1 May 2007. 12 January 2009 http://jama.ama-assn.org/cgi/content/full/287/17/2236.

5. Bacon, J.B. *Thermal Inactivation of Bacillus Anthracis using Micro-Etched Platforms and Carbon Black.* MS thesis, AFIT/GWM/ENP/09-M01. Graduate School of Engineering and Management, Air Force Institute of Technology (AU), Wright-Patterson AFB OH, March 2009.

6. Baker, W.P. Class Notes, MTH 605, Nonlinear Differential Equations. Graduate School of Engineering and Management, Air Force Institute of Technology (AU), Wright-Patterson AFB OH, Spring Quarter 2008.

7. Baker, W.P., and Burggraf, L.W. "Spore Thermal Inactivation Model," *AFNWCA Briefing.* Air Force Institute of Technology (March 2008).

8. Beaman, T.C., Greenamyre, J.T., Corner, T.R., Pankratz, H.S., and Gerhardt, Peter. "Bacterial Spore Heat Resistance Correlated with Water Content, Wet Density, and Protoplast/Sporoplast Volume Ratio," *Journal of Bacteriology,* 150: 870-877 (May 1982).

9. Carslaw, H.S. and Jaeger, J.C. *Conduction of Heat in Solids (2nd Edition).* New York: Oxford University Press, 1959.

10. Chapman, A.J. *Heat Transfer (3rd Edition).* New York: Macmillan Publishing Co., 1974.

11. Coleman, W.H., Chen, D., Li, Y., Cowan, A.E., and Setlow, P.. "How Moist Heat Kills Spores of *Bacillus subtilis*," *Journal of Bacteriology,* 189: 8458-8466 (December 2007).

12. Covington, A.K., Bates, R.G., and Durst, R.A. "Definition of pH scales, standard reference values, measurement of pH and related terminology," *Pure and Applied Chemistry,* 57: 531542 (1985).

13. Crick, F.H.C. "On the Genetic Code," *Science,* 139: 461-464 (1963).

14. Del Nobile, M.A., Buonocore, G.G., Palmieri, L., Aldi, A., and Acierno, D. "Moisture transport properties of polyamides copolymers intended for food packaging applications," *Journal of Food Engineering,* 53: 287-293 (2002).

15. Doughty, A., and Mackie, J.C. "Kinetics of Thermal Decomposition of the Diazines: Shock-tube Pyrolysis of Pyrimidine," *Journal of the Chemical Society, Faraday Transactions,* 90: 541-548 (1994).

16. Driks, A. "The *Bacillus subtilis* spore coat," *Microbiology and Molecular Biology Reviews,* 63: 1-20 (March 1999).

17. Fernelius, A.L., Wilkes, C.E., DeArmon, I.A., and Lincoln, R.E. "A Probit method to interpret thermal inactivation of bacterial spores," *Journal of Microbiology*, 75: 300-304. (1958).

18. Geeraerd, A.H., Herremans, C.H., and Van Impe, J.F. "Structural model requirements to describe microbial inactivation during a mild heat treatment," *International Journal of Food Microbiology*, 59: 185-209 (May 2000).

19. Gerhardt, P.C. and Marquis, R.E. "Spore thermoresistance mechanisms," *Regulation of Prokaryotic Development*, Washington DC: American Society for Microbiology, (1989).

20. Goetz, K.M. *Lethality of Bacillus Anthracis Spores Due to Short Duration Heating Measured Using Infrared Spectroscop.* MS thesis, AFIT/GNE/ENP/05-04. Graduate School of Engineering and Management, Air Force Institute of Technology (AU), Wright-Patterson AFB OH, March 2005.

21. Hawkins, L.S. *Micro-Etched Platforms for Thermal Inactivation of Bacillus Anthracis and Bacillus Thuringiensis Spores*. MS thesis, AFIT/GWM/ENP/08-M01. Graduate School of Engineering and Management, Air Force Institute of Technology (AU), Wright-Patterson AFB OH, March 2008.

22. Holwitt, E., Kiel, J. L., Alls, J. L., Morales, P. J., and Gifford, H. "Thermal sensitivity of biowarfare simulants," *Chemical and Biological Sensing, Proceedings of SPIE,* 4036: 31-39 (April 2000).

23. Ishihara, Y., Takano, J., Mashimo, S., and Yamamura, M. "Determination of water necessary for survival of *Bacillus subtilis* vegetative cells and spores," *Thermochimica Acta,* 235: 153-160 (1994).

24. Jagannath, A., Tsuchido, T., and Membre, J.-M. "Comparison of the thermal inactivation of *Bacillus subtilis* spores in foods using the modified Weibull and Bigelow equations," *Food Microbiology,* 22: 233-239 (2000).

25. Leveque, R.J. *Finite Volume Methods for Hyperbolic Problems.* Cambridge, UK: Cambridge University Press, 2002.

26. Lindahl, T., and Nyberg, B. "Heat-Induced Deamination of Cytosine Residues in Deoxyribonucleic Acid," *Biochemistry,* 13: 3405-3410 (1974).

27. McNaught, A.D. and Wilkinson, A. *International Union of Pure and Applied Chemistry, Compendium of Chemical Terminology, (2nd edition).* Oxford: Blackwell Scientific Publications, 1997.

28. Melly, E., Genest, P.C., Gilmore, M.E., Little, S., Popham, D.L., Driks, A., and Setlow, P. "Analysis of the properties of spores of *Bacillus subtilis* prepared at different temperatures," *Journal of Applied Microbiology,* 92: 1105-1115 (2000).

29. Meot-Ner (Mautner), Michael, Dongre, Ashok R., Somogyi, Arpad, and Wysocki, Vicki H. "Thermal Decomposition Kinetics of Protonated Peptides and Peptide Dimers, and Comparison with Surface-induced Dissociation," *Rapid Communications in Mass Spectrometry,* 9: 829-836 (1995).

30. Mohr, P.J., Taylor, B.N., and Newell, D.B. "CODATA Recommended Values of the Fundamental Physical Constants: 2006," *Review of Modern Physics,* 80: 633730 (December 2007).

31. Morton, K. W. and Mayers, D. F. *Numerical Solutions of Partial Differential Equations (2nd Edition).* Cambridge UK: Cambridge University Press, 2005.

32. Murray, J.D. *Mathematical Biology I: An Introduction (3rd Edition).* New York: Springer-Verlag, 2002.

33. Nellis, G.F., and Klein, S.A. *Intermediate Heat Transfer with Software Tools.* Madison WI: Cambridge University Press, 2002.

34. Orsburn, B., Melville, S.B., and Popham, D.L. "Factors Contributing to Heat Resistance of *Clostridium perfringens* Endospores," *Applied and Environmental Microbiology,* 74: 3328-3335 (June 2008).

35. Rosenberg, B.H., Cavalieri, L.F., and Ungers, G. "The Negative Control Mechanism for E. Coli DNA Replication," *Proceedings of the National Academy of Sciences of the USA,* 63: 1410-1417 (1969).

36. Rubinow, S.I. *Introduction to Mathematical Biology.* New York: John Wiley and Sons, 1975.

37. Schleif, Robert F. *Genetics and Molecular Biology.* Reading MA: Addison-Wesley Publishing Company, 1985.

38. Seebaugh, W.R., and Hanson, R.F. "Response of Bacterial Spores to Weapon Environments," Science and Engineering Associates, Inc. Alexandria, VA: Defense Special Weapons Agency, (June 1997).

39. Setlow, P. "Bacterial Stress Responses," *Bacterial Stress Responses.* Washington DC: American Society for Microbiology, (2000).

40. Setlow, P. "Spores of Bacillus subtilis: their resistance to and killing by radiation, heat and chemicals," *Journal of Applied Microbiology,* 101: 514-525 (2006).

41. Smelt, J.P.P.M., Hellemons, J.C., Wouters, P.C., and van Gerwen, S.J.C. "Physiological and mathematical aspects in setting criteria for decontamination of foods by physical means," *International Journal of Food Microbiology,* 78: 57-77 (2002).

42. "Soda Lime Glass," CiDRA Precision Services, LLC, 2008. 21 August 2008 http://www.cidracps.com/pm/materials/soda-lime.html.

43. Spang, B. "U in Heat Exchangers," Online Chemical Engineering Information, 2008. 6 February 2009 http://www.cheresources.com/uexchangers.pdf.

44. Spotts-Whitney, E. A., Beatty, M.E., Taylor, T.H., Weyant, R., Sobel, J., Arduino, M.J., and Ashford, D.A. "Inactivation of *Bacillus anthracis* Spores," *Emerging Infectious Diseases,* 101 (June 2003).

45. Wackerly, D.D., Mendenhall, W. III, and Scheaffer, R.L. *Mathematical Statistics with Applications (Sixth Edition).* U.S.A.: Duxbury, 2002.

46. Westphal, A.J., Price, P.B., Leighton, T.J., and Wheeler, K.E. "Kinetics of size changes of individual *Bacillus thuringiensis* spores in response to changes in relative humidity," *Proceedings of the National Academy of Sciences of the USA,* 100: 3461-3466 (18 March 2003).

47. Xu, S., Labuza, T.P., and Diez-Gonzalez, F. "Inactivation of *Bacillus anthracis* Spores by a Combination of Biocides and Heating under High-Temperature Short-Time Pasteurization Conditions," *Applied and Environmental Microbiology*, 74: 3336-3341 (June 2008).

48. Yoshii, H., Furuta, T., Noma, S., and Noda, T. "Kinetic Analysis of Soy-protein Denaturation by a Temperature programmed Heat-denaturation Technique," *Agricultural and Biological Chemistry*, 54: 863-869 (1990).

REPORT DOCUMENTATION PAGE

Form Approved
OMB No. 0704–0188

1. REPORT DATE *(DD–MM–YYYY)*	2. REPORT TYPE	3. DATES COVERED *(From — To)*
26-03-2009	Master's Thesis	June 2008–March 2009

4. TITLE AND SUBTITLE

Modeling Thermal Inactivation of *Bacillus* Spores

5a. CONTRACT NUMBER

5b. GRANT NUMBER

5c. PROGRAM ELEMENT NUMBER

6. AUTHOR(S)

Knight, Emily A. Captain, USAF

5d. PROJECT NUMBER

5e. TASK NUMBER

5f. WORK UNIT NUMBER

7. PERFORMING ORGANIZATION NAME(S) AND ADDRESS(ES)

Air Force Institute of Technology
Graduate School of Engineering and Management (AFIT/EN)
2950 Hobson Way, Building 640
WPAFB OH 45433-8865

8. PERFORMING ORGANIZATION REPORT NUMBER

AFIT/GAM/ENC/09-01

9. SPONSORING / MONITORING AGENCY NAME(S) AND ADDRESS(ES)

Ms. Angelica Rubio, Combating WMD Flight
709th Armament Systems Squadron
Kirtland Air Force Base, NM

10. SPONSOR/MONITOR'S ACRONYM(S)

11. SPONSOR/MONITOR'S REPORT NUMBER(S)

12. DISTRIBUTION / AVAILABILITY STATEMENT

APPROVED FOR PUBLIC RELEASE, DISTRIBUTION UNLIMITED

13. SUPPLEMENTARY NOTES

14. ABSTRACT This research models and analyzes methods to damage *Bacillus anthracis* spores through heat treatment. AFIT researchers have developed methods to characterize the effects of heating spores to high temperatures and for short durations similar to the thermal pulse of conventional weapon detonation. This research models the current experiment and evaluates the rate of thermal diffusion throughout the spores. A micro-model of the effects of dry and wet heating on a spore is presented. Heating a spore energizes adsorbed, absorbed, and chemically bound water molecules. These energized molecules have greater mobility within the spore, as well as between the spore and the surrounding environment. The water release permits hydrolysis reactions to occur with the spore's DNA and proteins. This degrades the DNA and proteins to such an extent that the DNA cannot replicate, thus causing spore death. We assert that spore damage is based on an initial DNA information content and the spore population's protein fitness. Once this protein fitness level is degraded below a critical value, the DNA cannot be repaired. A probability of kill model based on water mobility, hydrolysis, a spore's DNA information content, and the spore population's protein fitness.

15. SUBJECT TERMS

spore, *Bacillus*, anthrax, thermal damage, hydrolysis

16. SECURITY CLASSIFICATION OF:			17. LIMITATION OF ABSTRACT	18. NUMBER OF PAGES	19a. NAME OF RESPONSIBLE PERSON
a. REPORT	b. ABSTRACT	c. THIS PAGE			William P. Baker, Ph.D, AFIT
U	U	U	UU	95	19b. TELEPHONE NUMBER *(include area code)* (937) 255-3636 x4517, William.Baker@afit.edu